Article published online: 2024-03-11

THIEME OPEN ACCESS

Review Article

Pearls and Pitfalls in Applying PI-RADS 2.1

Ankur Pandey[1] Soumyadeep Ghosh[1] Priyanka Prajapati[1] Nabih Nakrour[1] Mukesh Harisinghani[1]

[1] Abdominal Imaging, Massachusetts General Hospital, Boston, Massachusetts, United States

Address for correspondence Ankur Pandey, MD, Room 270, White Building, Massachusetts General Hospital, 55 Fruit St, Boston, MA 02114, United States (e-mail: apandey8@mgh.harvard.edu).

J Gastrointestinal Abdominal Radiol ISGAR

Abstract

The use of Prostate Imaging Reporting and Data System (PI-RADS) with multiparametric magnetic resonance imaging (MRI) has significantly improved the detection of clinically significant prostate cancer (csPCa), but there are certain challenges that the reader may face. This review provides an overview of the pitfalls associated with the PI-RADS system for multiparametric prostate MRI (mpMRI), with suggestions/pearls to help overcome these pitfalls.

PI-RADS assessment is hindered by several causes of false positives (FPs) and false negatives (FNs). In addition, there is wide variability in the positive predictive value (PPV) of the PI-RADS system across different centers, highlighting the need for improvement. While the negative predictive value (NPV) for csPCa is generally high, variations exist.

This review discusses the pitfalls contributing to FNs, including MRI artifacts, such as susceptibility and motion artifacts. Techniques to optimize image acquisition, such as switching the phase encoding direction and reducing bowel peristalsis, are suggested to mitigate these artifacts. Improper *b*-value selection for diffusion-weighted imaging (DWI) is another pitfall, emphasizing the importance of using high *b*-values ($\geq$1,400 s/mm^2) to optimize neoplasm detection. Similarly, optimizing window settings to visualize csPCa, correctly positioning the endorectal coil, awareness of rare variants like mucinous adenocarcinoma and cribriform adenocarcinoma, and distinguishing central zone tumors from normal central zone are discussed.

This article highlights the common pitfalls causing FPs, such as benign pathologies like prostatitis, granulomatous prostatitis, prostatic abscess, stromal BPH nodules, extruded BPH nodules, and prostatic calcifications. It also discusses the pitfalls related to normal anatomical structures, including the central zone, anterior fibromuscular stroma, thickened surgical capsule, neurovascular bundle, and periprostatic venous plexus. Techniques for carefully evaluating these entities' morphology and distribution of signal abnormalities are described to avoid overdiagnosing these as PCa. The article also addresses the pitfalls related to postintervention changes, including postbiopsy hemorrhage and artifacts caused by the UroLift procedure, while providing recommendations for managing these challenges.

Finally, the pitfalls that may be encountered during staging, including evaluation for extraprostatic extension, and pelvic nodal and osseous metastases, are highlighted.

Keywords

- magnetic resonance imaging
- mpMRI
- prostate
- prostatic neoplasms
- prostatitis
- prostatic hyperplasia

DOI https://doi.org/10.1055/s-0043-1778636.
ISSN 2581-9933.

Thieme Medical and Scientific Publishers Pvt. Ltd., A-12, 2nd Floor, Sector 2, Noida-201301 UP, India

Introduction/Background

Advancements in prostate magnetic resonance imaging (MRI), along with the Prostate Imaging Reporting and Data System (PI-RADS) scoring system, have changed the management of prostate cancer (PCa). Initial clinical guidelines in 2012 for multiparametric prostate MRI (mpMRI) included the original PI-RADS reporting system.[1] This was followed by an updated PI-RADS version 2 in 2015 and another update, PI-RADS version 2.1, in 2019.[2] These guidelines have profoundly impacted the detection of PCa, particularly clinically significant PCa (csPCa), with a recent meta-analysis showing a 94% accuracy of mpMRI for csPCa.[3]

However, the utility of the PI-RADS scoring system is limited by false positives (FPs) and false negatives (FNs), lowering the positive predictive value (PPV) and negative predictive value (NPV). A recent large multicenter study demonstrated PPV of 35% (interquartile range [IQR], 27–44%) for a PI-RADS score $\geq$3/5 and 49% (IQR, 27–48%) for a PI-RADS score $\geq$4/5.[4] Thus, the PPV was low and varied widely across centers. The NPV of mpMRI is higher in comparison, with a meta-analysis showing an NPV of 88.1% (IQR, 85.7–92.3) for csPCa,[5] with negative defined as PI-RADS categories 1 and 2. Of note, the definition of positive mpMRI has varied in the literature as a score $\geq$3/5 or $\geq$4/5. PPV and NPV influence the test's utility and affect decision-making. Therefore, this review aims to highlight some pitfalls that are the common cause of FP and FN, which, if avoided, could improve the test's utility.

Discussion

PI-RADS version 2.1 has defined the primary sequences used in determining the overall suspicion for csPCa (dominant sequence) for the peripheral and transition zones (TZs). The abnormalities on the dominant sequence for a respective zone carry higher weightage. For the peripheral prostate zone (PZ), apparent diffusion coefficient (ADC) map with diffusion-weighted imaging (DWI) utilizing high *b* values ($\geq$1,400 s/mm^2) is the dominant sequence. The dominant sequence for the TZ is the T2-weighted imaging (T2WI). A mimic or pitfall affecting a particular zone on its dominant sequence has a higher potential of causing diagnostic confusion within that zone.

Pitfalls Causing False Negatives (FNs)

FNs Related to MRI Technique

Pitfalls related to the MR technique are primarily seen in association with diffusion imaging. While allowing rapid acquisition, DWI also warrants technique optimization due to extreme sensitivity to susceptibility and motion. It is often performed as an axial-free breathing echo-planar technique combined with spectral fat saturation.

- *Susceptibility and motion artifacts*: DWI acquisition with echo-planar imaging (EPI) involves rapidly changing strong magnetic field gradients. This can induce superimposed magnetic fields via the induction of eddy current, which can ultimately cause anatomical distortion of the prostate structures compared to the T2WI. Sources of magnetic field heterogeneity, such as gas, calcium, or metal in the prostate region, worsen this problem (►**Fig. 1A–F**). This can present as stretching and distortion of the prostate boundary, surgical capsule, or focal lesions, along with shape deformation and spatial misregistration. Similar anatomical distortion can occur with motion, often related to rectal peristalsis, affecting the T2WI and DWI sequences.

Pearls

Image acquisition, particularly DWI, can be optimized to mitigate the above-described artifacts. The phase encoding direction can be switched routinely to side to side for DWI to avoid propagation of the artifacts related to rectal stool/gas onto the prostate (►**Fig. 1G–J**). This contrasts the routinely performed anterior to posterior phase encoding in the pelvic MRI based on relatively shorter pelvic dimension than side to side. Patients may also be encouraged to evacuate the rectum or enema may be considered just before the MRI to reduce the artifacts from gas, stool, and peristalsis. Occasionally, placing rectal catheters to remove gas or administering water-based gel can help if susceptibility from stool or gas still degrades the examination. Although bowel peristalsis can be reduced by using antispasmodic agents such as glucagon or hyoscyamine, their use is not essential; it needs to be weighed against the increased costs and potential side effects.[6] Utilizing 1.5-T MRI instead of the 3-T MRI can specifically be considered in patients with pelvic metal prostheses (e.g., hip arthroplasty) to reduce the associated susceptibility artifacts.

- *Improper b-value selection for DWI*: While *b*-values of up to 1,000 s/mm^2 are often sufficient in most DWI assessments of abdominopelvic organs, the background benign prostate parenchyma is not sufficiently suppressed on such *b*-values to allow optimal neoplasm detection. The utility of high *b*-values in the 1,400 to 2,000 s/mm^2 range has been demonstrated in optimizing the conspicuity of csPCa,[7] most of which restrict diffusion, allowing them to appear sufficiently hyperintense relative to the background parenchyma.

Pearls

A high *b*-value ($\geq$1,400 s/mm^2) image set is mandatory per the PI-RADS committee recommendations, with a *b*-value of 1,600 to 2,000 s/mm^2 often preferred.[7] Low (0–100 s/mm^2) and intermediate (800–1,000 s/mm^2) *b*-values are utilized for ADC calculation. The required high *b*-value ($\geq$1,400 s/mm^2) can either be calculated from the low/intermediate *b*-values or acquired separately. However, the high *b*-value DWI should not be included in the ADC map generation to avoid diffusion kurtosis effect on ADC, resulting in lower-than-expected ADC.

- *Suboptimal viewing of DWI/ADC*: The PI-RADS criteria for DWI/ADC maps are based on qualitative visual

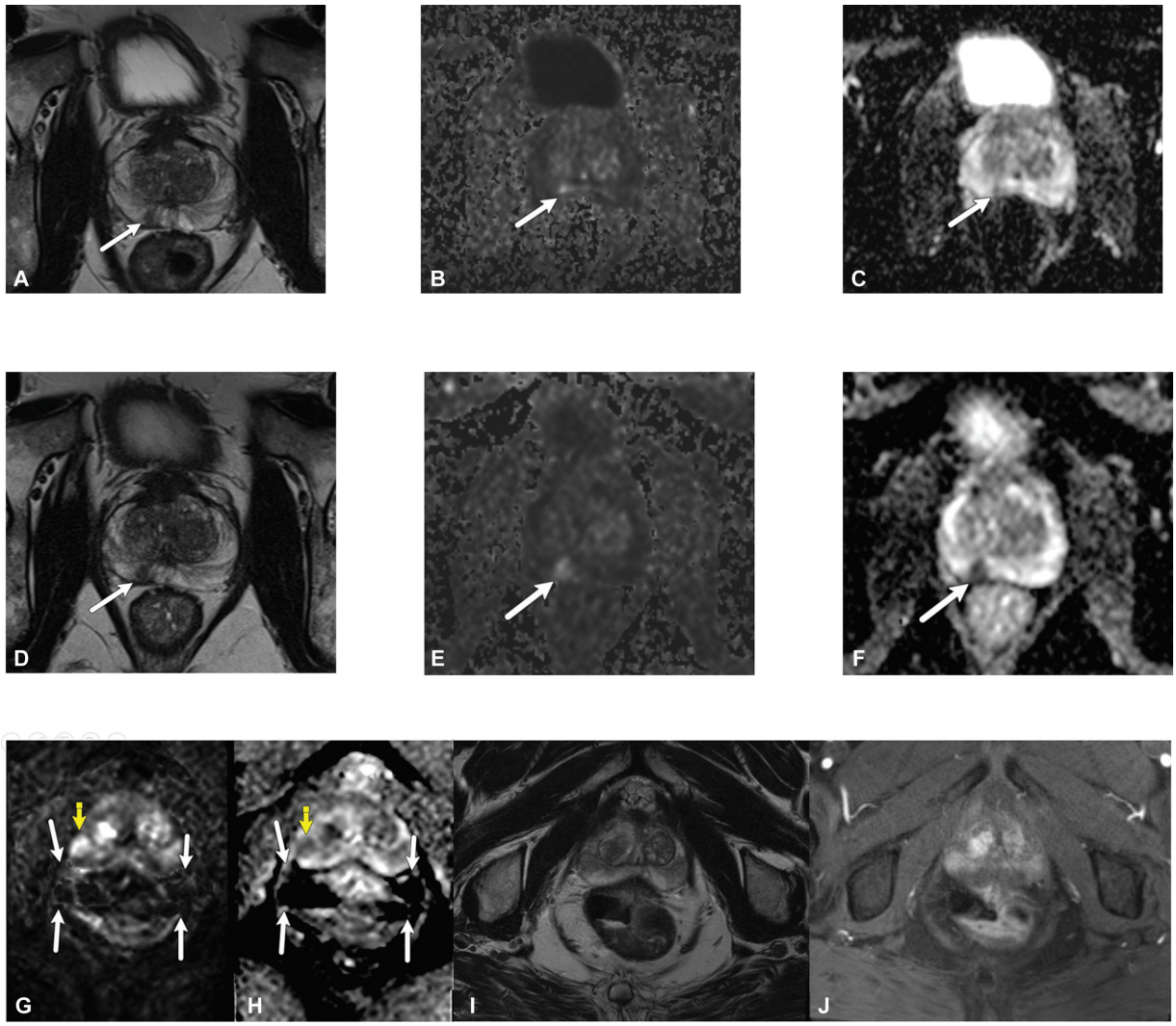

Fig. 1 (**A**) Axial T2-weighted image (T2WI; *arrow*) shows a focal lesion exhibiting moderate hypointensity in the right mid-gland prostate zone (PZ). (**B**) Diffusion-weighted imaging (DWI; *arrow*) and (**C**) apparent diffusion coefficient (ADC) map (*arrow*) show no discrete corresponding DWI hyperintense or ADC hypointense abnormality; however, it can be seen that the susceptibility artifact from rectal gas degrades the assessment of the most posterior aspect of the PZ. (**D**) On subsequent magnetic resonance imaging (MRI), axial T2WI (*arrow*) shows a similar focal lesion, which is now clearly noted to exhibit marked diffusion restriction on DWI (*arrow*) and (**F**) ADC map (*arrow*). Biopsy showed Gleason 3 + 4 prostate cancer (PCa) in the right mid-gland. In another patient, there is a band of artifacts related to rectal stool and gas (*white arrows*) seen extending horizontally on both (**G**) DWI and (**H**) ADC. Since DWI was performed with the phase encoding direction switched side to side as part of routine prostate imaging protocol, this prevented the band of artifact from propagating onto the prostate, which could have otherwise obscured the diffusion-restricting PI-RADS 4 lesion (*yellow arrows* in **G** and **H**) exhibiting (**I**) focal hypointensity on T2WI with (**J**) early enhancement. The T2 hypointense area in the left PZ was considered a postinflammatory change considering the well-demarcated margins.

assessment. Optimal assessment requires that these sequences be viewed with consistently similar contrast. Notably, the default window settings on the picture archiving and communication system (PACS) may not allow the tumor to be sufficiently conspicuous from the background parenchyma.

Pearls

Due to the variable DWI acquisition technique, the optimal window settings may need to be determined for each system. The window level and width settings of 1,400/1,400 for the ADC map may be used as a starting point, but this may not be ideal for all systems. The levels should be adjusted to visualize csPCa as markedly hyperintense on high *b*-value DWI and markedly hypointense on ADC maps. A quantitative ADC threshold of less than 750 to 900 $\mu m^2/s$ may help differentiate malignant from benign tissue in PZ (lower value favoring csPCa).[8] However, the routine clinical utility of such thresholds is limited by the potential technical variability of ADC and overlap of ADC between benign and malignant lesions.

- *Artifacts related to the use of endorectal coil (ERC)*: Using an ERC is optional based on the PI-RADS recommendations. Surface coils with a sufficiently high number of external phased array coil elements and radiofrequency (RF) channels (16 or more) can provide adequate signal-to-noise ratio (SNR)/image quality without ERC, even with 1.5-T MRI. However, ERC can increase the SNR at any MR field

strength. It can be advantageous, such as in some older 1.5-T MR systems, with larger patients where SNR is limited with external coils alone or where particularly high spatial resolution is desired for staging purposes. Besides the time, patient preference, and cost considerations, ERC use is associated with gland deformation and additional artifacts. ERC balloons utilizing air can introduce another source of susceptibility artifacts. Improper placement of the ERC antenna can cause artifacts mimicking malignancy.

Pearls

ERC should be positioned in a plane perpendicular to the side-to-side phase encoding direction to avoid artifactual focal diffusion restriction on DWI and enhancement adjacent to the coil. Since these artifacts do not affect T2WI and ADC map, correlating with these sequences will also avoid mislabeling these findings as pathologic. It is recommended that the ERC antenna be placed from the 10 o'clock position to the 2 o'clock position. ERC balloon alternatives without air are available to prevent associated susceptibility.

FNs Related to Variants and Unusual Patterns of Prostate Malignancies

- *Mucinous adenocarcinoma*: The mucinous subtype of prostate adenocarcinoma is rare, accounting for approximately 0.4% of all prostate adenocarcinomas.[9] It is diagnosed when greater than 25% of the tumor contains clustered cells floating in mucin lakes. Imaging diagnosis is challenging since appearance deviates from the typical nonmucinous adenocarcinoma. Thus, conventional PI-RADS-based interpretation designed for nonmucinous PCa fails to be applied to mucinous adenocarcinoma. The tumor's mucinous content leads to hyperintensity on T2WI, resembling cystic BPH, abscess, or other benign lesions. Unlike typical adenocarcinoma, it usually does not exhibit diffusion restriction. Although it may appear hyperintense on high *b*-value DWI, minimal to no hypointensity is observed on ADC maps.[10] In some cases, mucinous adenocarcinoma can present as isointense with the normal PZ tissue.[11] Diagnosis remains challenging even with biopsy due to the paucity of cells obtained. Therefore, it is crucial to be aware of this rare variant and recognize the appearance of this entity on MRI.

Pearls

The typical appearance of multilocular cystic mass with T2 hyperintensity and dynamic contrast-enhanced (DCE) MRI showing enhancing septations should raise suspicion for this rare subtype, even without diffusion restriction (►**Fig. 2**).

- *Cribriform adenocarcinoma*: Typical acinar morphology is observed in over 90% of PCa.[9] However, a predominant cribriform morphology exists among the spectrum of variants of prostatic adenocarcinoma and impairs csPCa detection.[12] In a study, predominant cribriform morphology accounted for 22% of patients with csPCa that had negative mpMRI,[5] with another study demonstrating that only 17% of cribriform histologic tumor types were detected on imaging.[9] Yet others have suggested a high detection rate of PCa with cribriform patterns.[13] Our own experience suggests that these lesions may be difficult to detect, particularly if the technique is not optimal or if the reader has limited experience. This difficult detection is possibly related to sparse cellular structure with higher

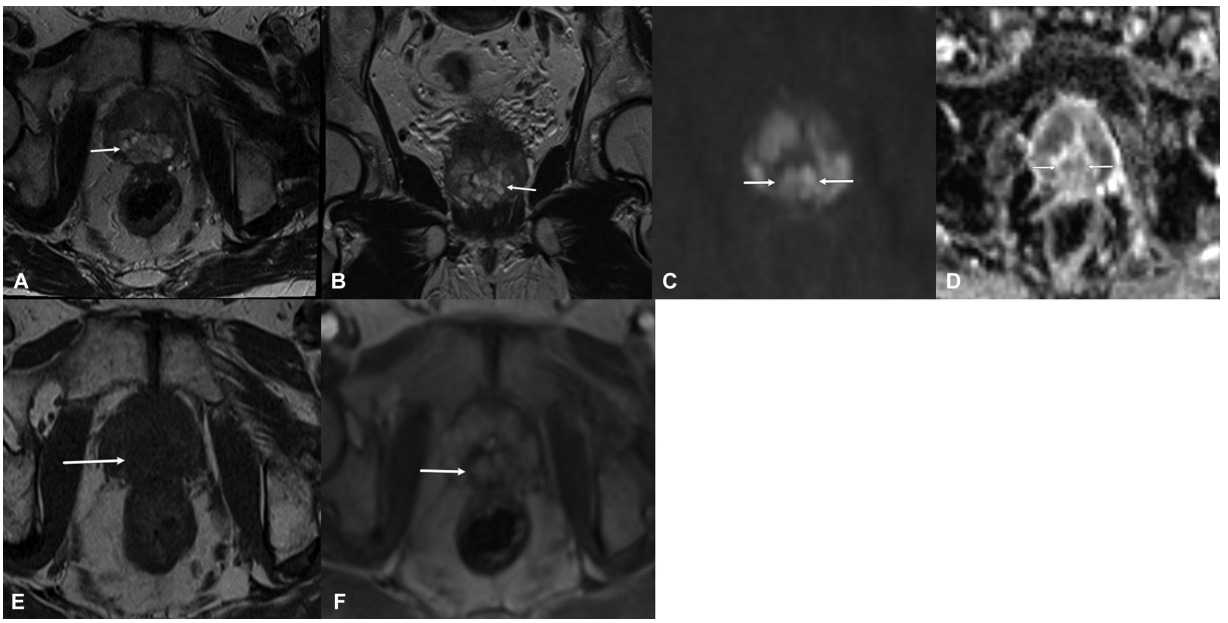

Fig. 2 (**A**) Axial and (**B**) coronal T2-weighted images (T2WIs) show a heterogeneous T2 hyperintense mass involving the bilateral posterior peripheral zone (PZ; *arrow*). The lesion does not restrict diffusion, as evidenced by the absence of (**C**) hyperintensity on diffusion-weighted imaging (DWI; *arrow*) or hypointensity on (**D**) apparent diffusion coefficient (ADC) map (*arrow*), different from the background adjacent PZ. Lesion exhibits (**E**) hypointensity on T1WI (*arrow*) with (**F**) early arterial enhancement on DCE (*arrow*). Prostate biopsy showed adenocarcinoma up to Gleason score $4+5=9$ with mucinous features.

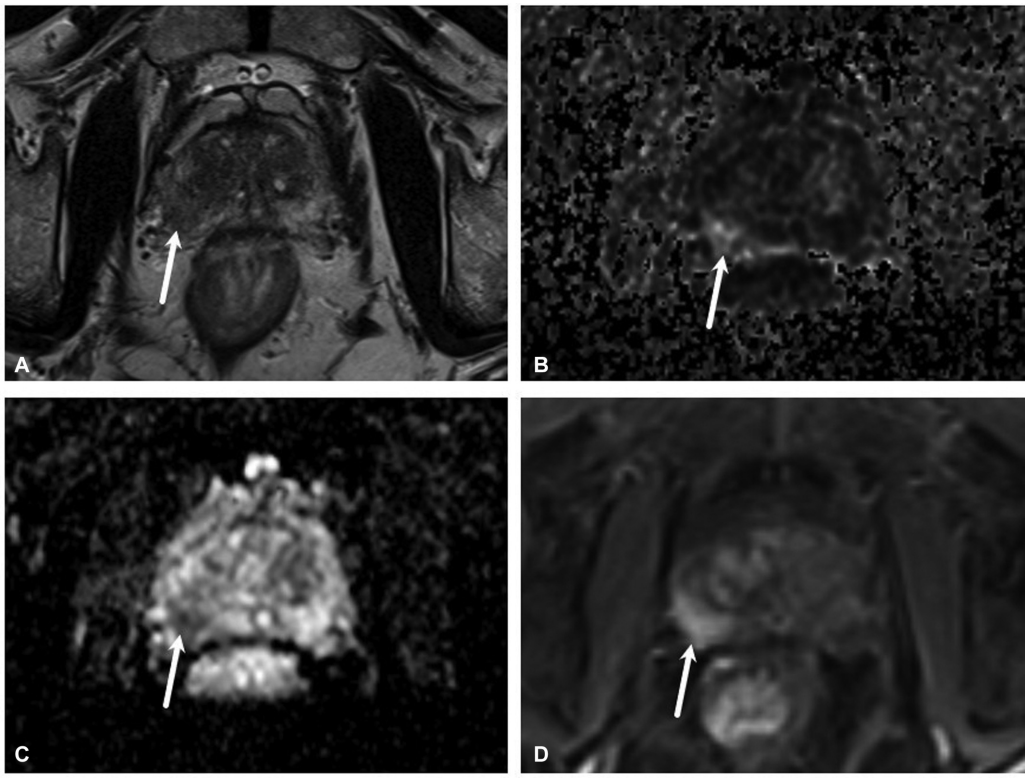

Fig. 3 (**A**) Axial T2-weighted image (T2WI; *arrow*) shows a focal area of mild to moderate hypointensity in the right peripheral zone (PZ). There is corresponding moderate diffusion restriction with (**B**) heterogeneous stippled hyperintensity on high *b*-value diffusion-weighted imaging (DWI; *arrow*) and (**C**) hypointensity on apparent diffusion coefficient (ADC) map (*arrow*) with (**D**) positive early enhancement (*arrow*). Biopsy revealed Gleason 4 + 3 adenocarcinoma with a cribriform pattern.

water content, leading to higher T2 signal and less diffusion restriction (►**Fig. 3**). Detection is important given recent evidence of cribriform morphology to be an aggressive PCa pattern with higher cancer-specific mortality.[9]

Pearls

While no distinctive imaging features have been conclusively associated with this histologic subtype, some have suggested lower ADC values than tumors without these patterns.[10] However, this is yet to be confirmed and contrasts the findings mentioned above from others, suggesting less diffusion restriction of these lesions.

- *Diffuse high-grade tumor*: The appearance of diffuse high-grade cancer can be variable depending on cancer grade but can mimic prostatitis.

Pearls

Diffuse high-grade cancer tends to have lower signal intensity (SI) on T2WI and more marked diffusion restriction, resulting in lower SI on ADC and higher SI on DWI, compared to prostatitis. Another finding suggestive of infiltrative high-grade cancer is the loss of normal zonal anatomy with the obliteration of the surgical capsule (►**Fig. 4**).

Pitfalls Causing False Positives (FPs)

FPs Related to Benign Pathologies

- *Acute or chronic prostatitis*: This is the most common cause of FP finding for PCa.[14] Prostatitis can be acute or chronic and the signal abnormalities may suggest csPCa on any of the mpMRI sequences. They may include an area of hypointensity on T2WI, often in the PZ close to the anatomical capsule, with a corresponding area of hypointensity on the ADC map and early arterial enhancement on DCE MRI (►**Fig. 5**).

Pearls

Morphology of the signal abnormality is often helpful in classifying an otherwise suspicious signal abnormality as secondary to a benign inflammatory process. Inflammation or postinflammatory changes are usually linear, wedge-shaped, or non-mass-like instead of rounded, defined, mass-like areas of signal abnormality exhibited by the PCa. Distribution of the signal abnormality is often also helpful, with diffuse involvement suggesting inflammatory etiology as opposed to a focal signal abnormality typically seen with PCa. Another feature to keep in mind is the orientation of the abnormal signal. While the linear/bandlike shape of signal abnormality favors benignity, it should bridge the anatomical

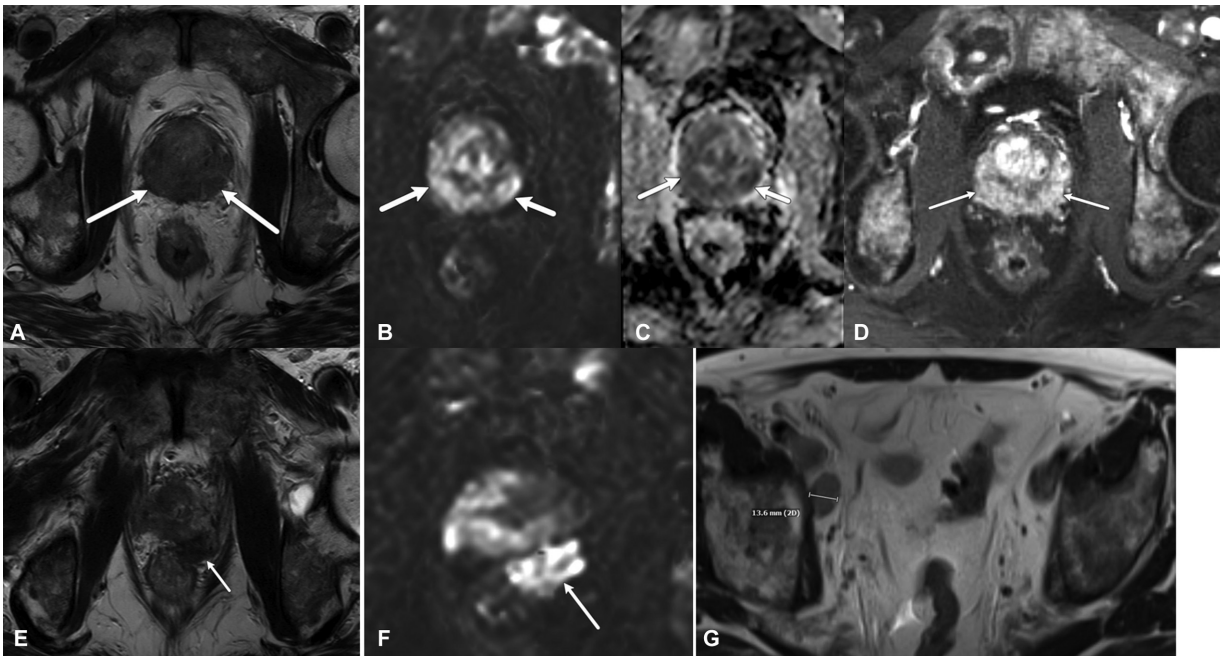

Fig. 4 There is diffuse infiltrative moderate hypointensity on (**A**) T2-weighted image (T2WI; *arrows*) throughout bilateral peripheral zones. There is corresponding marked diffusion restriction with marked (**B**) diffusion-weighted imaging (DWI) hyperintensity (*arrows*) and (**C**) apparent diffusion coefficient (ADC) hypointensity (*arrows*), with (**D**) early arterial enhancement (*arrows*). On T2WI (A), note the loss of zonal anatomy with obliteration of the surgical capsule between the peripheral zone (PZ) and transitional zone (TZ). Also note the (**E**) T2 hypointense (*arrow*), (**F**) DWI hyperintense diffusion restricting (*arrow*) extraprostatic extension obliterating the left rectoprostatic angle, with (**G**) pelvic lymphadenopathy (caliper). Prostate biopsy showed a total of 17/20 cores positive for up to Gleason 5 + 4 disease with 100% maximum involvement.

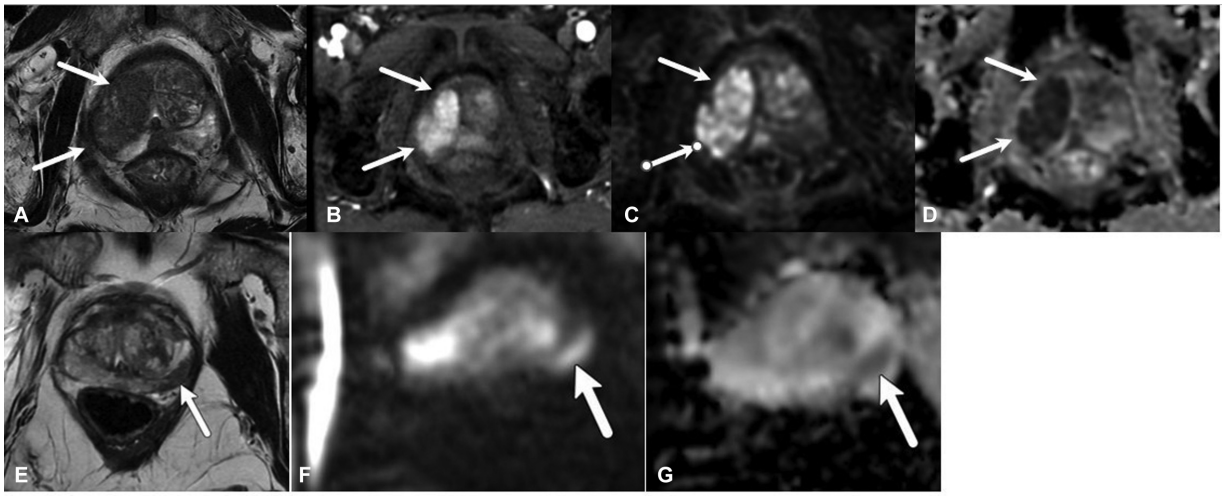

Fig. 5 Axial (**A**) T2-weighted image (T2WI; *arrows*) shows focal moderate hypointensity in the right peripheral zone (PZ) and transitional zone (TZ) with (**B**) early enhancement (*arrows*). There is corresponding marked diffusion restriction with (**C**) hyperintensity on high *b*-value diffusion-weighted imaging (DWI; *arrows*) and (**D**) hypointensity on apparent diffusion coefficient (ADC) map (*arrows*). Biopsy of this PI-RADS 5 lesion revealed prostatitis. In another patient, (**E**) a wedge-shaped hypointensity on T2WI (*arrow*) also exhibits marked diffusion restriction on (**F**) high *b*-value DWI (*arrow*) and (**G**) ADC map (*arrow*). A biopsy of this lesion showed Gleason 3 + 3 adenocarcinoma. Note that although the focal T2 hypointensity (*arrow* in **E**) is bandlike, it parallels the capsule rather than bridging anatomical and surgical capsules.

and surgical capsule rather than paralleling the capsule. Despite these differences, appearances can overlap, and sometimes, a confident differentiation between inflammation-related changes and csPCa may be difficult (►**Fig. 5**). In such instances, a reasonable approach may involve a targeted biopsy and a repeat MRI after 6 months or greater if the targeted biopsy demonstrates benign pathology. A decision may then be made regarding continued imaging surveillance or repeating the biopsy based on the appearance on follow-up imaging.

- *Granulomatous prostatitis*: While most cases of granulomatous prostatitis are idiopathic, we most likely see it secondary to intravesical bacillus Calmette–Guerin (BCG) therapy for urinary bladder cancer.[15] On mpMRI, this can demonstrate a discrete masslike appearance with

marked signal abnormalities, including hypointensity on T2WI and ADC, hyperintensity on DWI, and possibly periprostatic fat stranding mimicking extracapsular extension, falsely suggesting csPCa. The signal abnormalities are often more pronounced than those with other forms of infectious prostatitis,[16] such that often a biopsy is necessary to rule out malignancy (►**Fig. 6A–E**).

Pearls

A helpful clue that, if present, may suggest this diagnosis and avoid biopsy includes the presence of peripheral enhancement with the central nonenhancing necrotic region (►**Fig. 6F–I**).

While a masslike appearance of granulomatous prostatitis without central necrosis can be exceedingly difficult to

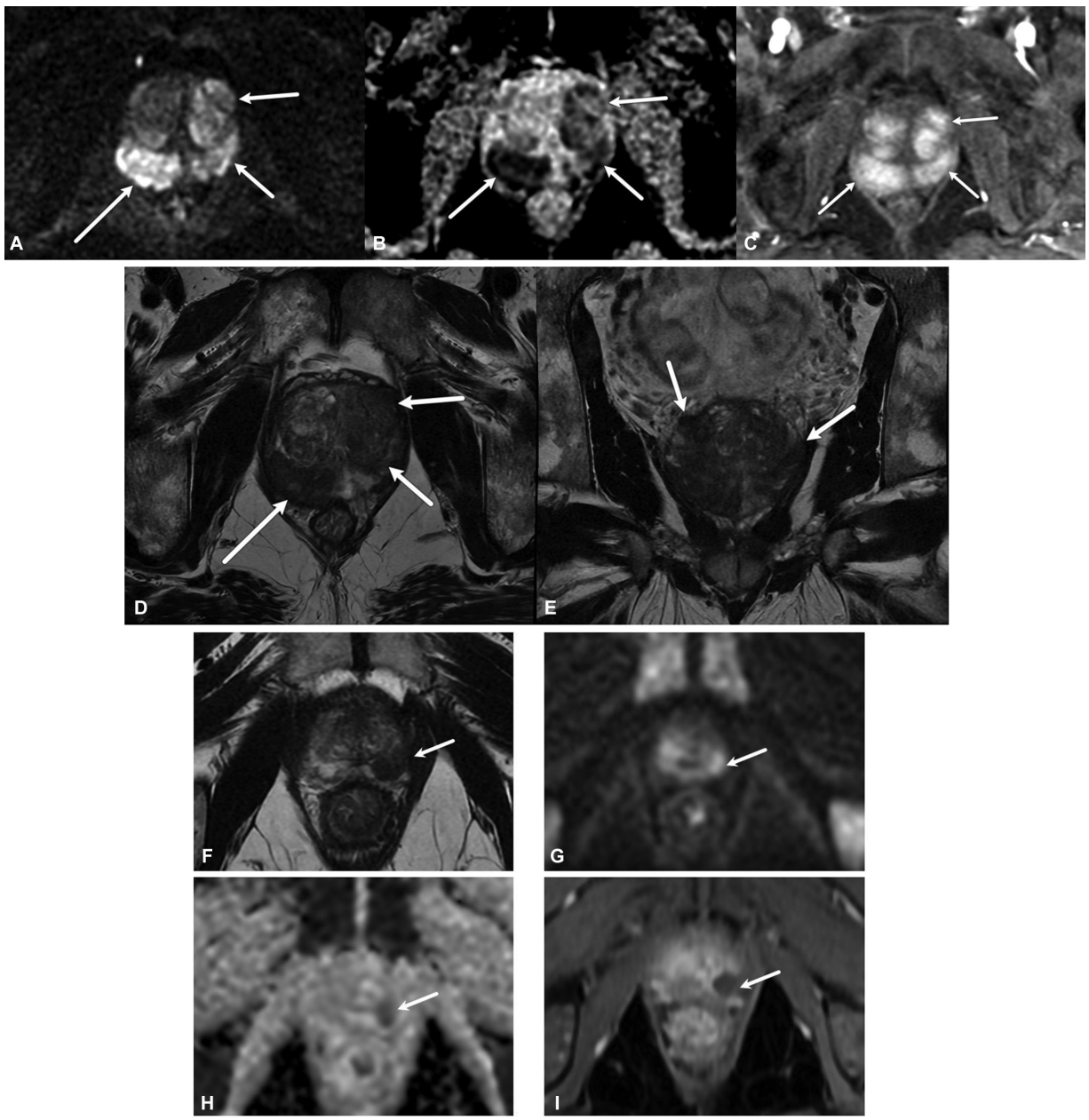

Fig. 6 Multifocal lesions in bilateral peripheral zone (PZ) and left transitional zone (TZ) exhibiting (**A**) marked hyperintensity on diffusion-weighted imaging (DWI; *arrows*), (**B**) marked hypointensity on apparent diffusion coefficient (ADC; *arrows*), and (**C**) positive DCE (*arrows*). (**D**) The lesions are homogenously hypointense on T2-weighted image (T2WI; *arrows*), with the left TZ lesion exhibiting moderate lenticular hypointensity. (**E**) There is broad-based capsular abutment, multifocal capsular bulging, and extracapsular extension cranially as seen on coronal T2WI (*arrows*), consistent with PI-RADS 5, and suspicious for multifocal clinically significant prostate cancers. Subsequent biopsy findings were consistent with nonspecific granulomatous prostatitis. In a different patient with a history of intravesical Bacillus Calmette–Guérin (BCG) therapy for urinary bladder cancer, (**F**) axial T2WI (*arrow*) shows a moderately hypointense lesion in the left PZ, with (**G**) corresponding marked diffusion restriction on high *b*-value DWI (*arrow*) and (**H**) ADC map (*arrow*). (**I**) However, note the absence of enhancement of the lesion (*arrow*), suggesting necrosis, which suggests BCG-related granulomatous prostatitis in this patient.

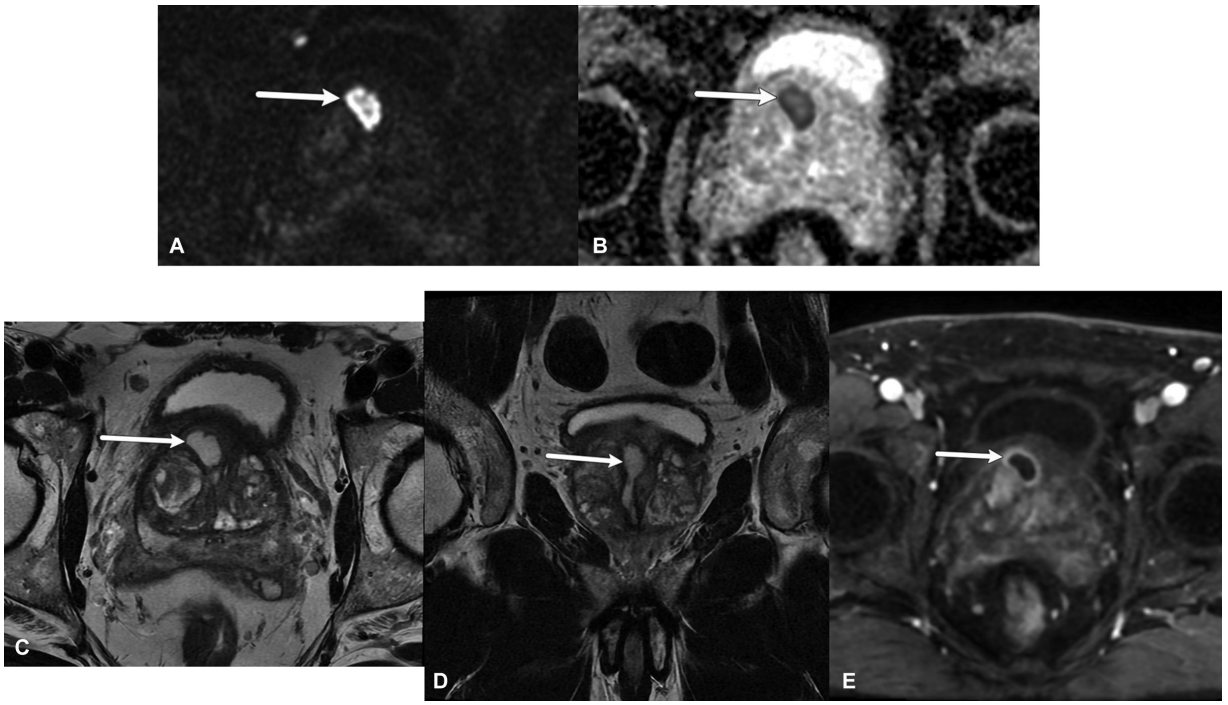

Fig. 7 Focal lesion in right anterior transitional zone (TZ) shows marked diffusion restriction with (**A**) marked hyperintensity on diffusion-weighted imaging (DWI; *arrow*) and (**B**) marked hypointensity on the apparent diffusion coefficient (ADC) map (*arrow*). Features suggestive of abscess were the patient's clinical setting, homogeneous central hyperintensity on (**C**) axial (*arrow*) and (**D**) coronal T2-weighted image (T2WI; *arrow*), with peripheral enhancement on (**E**) postcontrast T1WI (*arrow*).

differentiate from csPCa and may require histopathologic confirmation, a history of intravesical BCG therapy may be a clue toward diagnosing granulomatous prostatitis by increasing the pretest probability of this benign diagnosis.

- *Prostatic abscess*: A prostatic abscess may complicate acute bacterial prostatitis with a distinct clinical presentation of fever, dysuria, and digital rectal examination (DRE) eliciting tenderness even with gentle palpation, often with fluctuance.
  If imaging is desired based on clinical suspicion of complicated bacterial prostatitis, transabdominal ultrasound is preferred. The appearance is typical of abscesses at other sites, demonstrating a complex collection within the prostate exhibiting peripheral vascularity. If mpMRI is performed, imaging appearance of a typical abscess, including a circumscribed region of marked hyperintensity on high *b*-value DWI, with corresponding marked hypointensity on ADC,[17] may mimic csPCa based on PI-RADS assessment.

Pearls

The first clue suggesting a diagnosis of a prostatic abscess would be a typical clinical picture as described earlier. The imaging clues to diagnosing an abscess rather than PCa include hyperintense or heterogeneous hypointense signal on T2WI and peripheral enhancement on DCE (►**Fig. 7**).

- *Stromal BPH nodules in TZ*: Benign prostatic hyperplasia (BPH) results from benign proliferation of prostatic epithelial and stromal cells in the TZ.[18] The SI of BPH nodules on T2WI depends on the proportion of stromal versus glandular elements. A greater percentage of glandular elements leads to higher SI on T2WI related to higher fluid within glandular secretions.[19,20] BPH nodules may also often demonstrate a mixed stromal and glandular appearance reflected by a heterogeneous signal on T2WI. A characteristic feature of stromal BPH nodules is their T2 hypointensity, unlike the T2 hyperintense glandular BPH nodules. This hypointense appearance on T2WI can cause the stromal BPH nodules in the TZ to be spuriously deemed highly suspicious for csPCa. This problem is compounded by the often-heterogeneous multinodular appearance of the TZ in patients with BPH, which generally makes detecting TZ tumors more difficult than PZ tumors.[21] Up to 30% of PCas arise from the TZ[22] and are also more frequently missed during standard prostate biopsies,[23] necessitating their accurate identification on mpMRI.

Pearls

An important feature favoring BPH nodules over the TZ PCa is the presence of discrete margins and an oval or spherical shape. Furthermore, a T2 hypointense capsule and T2 hypointensity lower than expected from PCa can provide additional clues (►**Fig. 8**). Internal foci of T2 hyperintensity may be observed in some stromal BPH nodules, along with only mild diffusion restriction, sometimes only on ADC maps or DWI. Additionally, the enhancement of these nodules is typically similar to other benign nodules within the prostate, rather than appearing earlier and more robust than the rest of the prostate, which is characteristic of PCa.

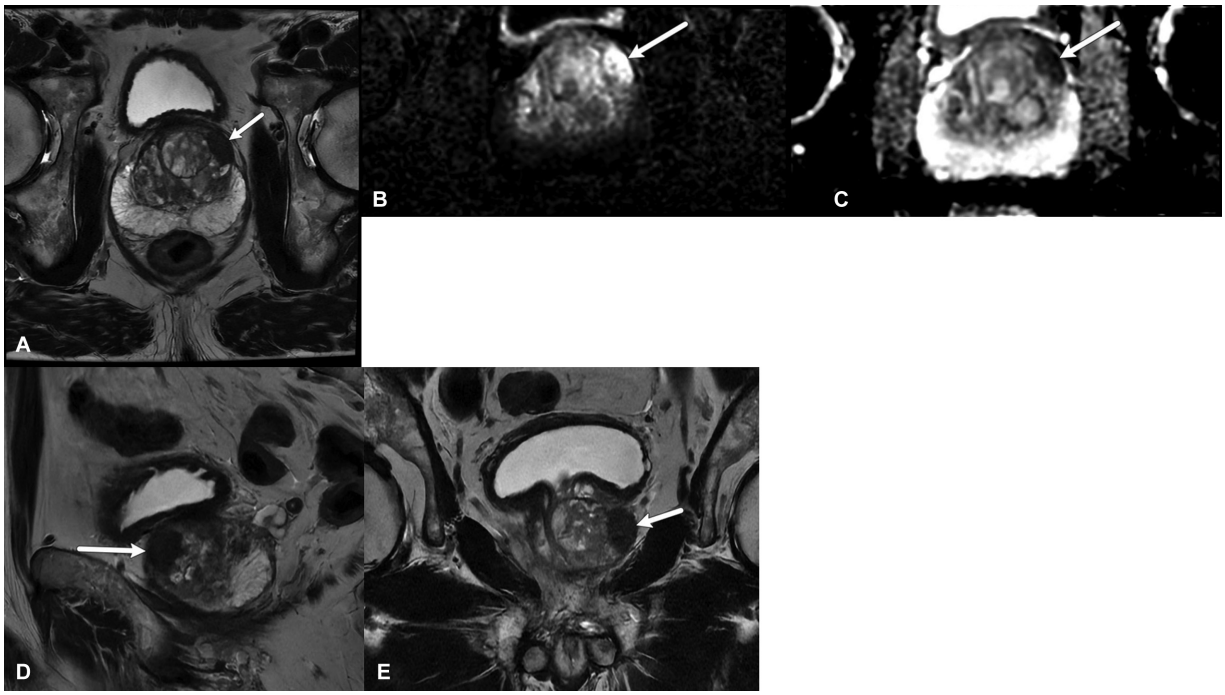

Fig. 8 Axial (**A**) T2-weighted image (T2WI; *arrow*) shows a lentiform homogenously hypointense focal lesion in the left anterior base transitional zone (TZ) exhibiting marked (**B**) diffusion restriction on diffusion-weighted imaging (DWI; *arrow*) and (**C**) apparent diffusion coefficient (ADC) map (*arrow*). The lesion's marked hypointensity and partial encapsulation, confirmed on (**D**) multiplanar T2W sagittal (*arrow*) and (**E**) coronal (*arrow*) images, suggest a stromal benign prostatic hyperplasia (BPH) nodule rather than a suspicious TZ lesion. This was correctly labeled as Prostate Imaging Reporting and Data System 2 (PI-RADS 2). A targeted prostate biopsy was subsequently performed and showed benign tissue.

This is usually in contrast to the noncircumscribed or lenticular shape, or irregular margins seen with TZ malignancy.[24,25] TZ malignancy can also be diagnosed when a clearly invasive behavior, such as extension into anterior fibromuscular stroma (AFS) or extraprostatic extension (EPE) is noted.

- *Extruded BPH nodules in the PZ*: Extruded BPH nodules in the PZ present a unique diagnostic challenge. These nodules result from the extension of BPH tissue from the TZ into the PZ and often abut the surgical capsule. They appear as focal nodules, often demonstrating hypointensity on T2WI that can show hyperintensity on high *b*-value DWI, hypointensity on ADC, and early enhancement. This appearance, especially that of a diffusion-restricting lesion in the PZ, mimics csPCa based on PI-RADS assessment.

Pearls

The presence of a capsule is extremely helpful in characterizing a typical BPH nodule. Another pearl is to utilize multiplanar T2WI, particularly sagittal and coronal planes. This can aid in identifying the capsule surrounding the nodule and demonstrate the continuity of the suspected signal abnormality with the BPH nodule arising from the TZ. Additionally, hyperintense foci on T2WI corresponding to the dilated acini may suggest extruded BPH nodules over PCa. These findings can increase diagnostic confidence and prevent overdiagnosing ectopic BPH nodules as malignancy (►**Fig. 9A–F**).

A pseudo-capsule can rarely form around PCa related to compressive or reactive peritumoral fibrosis, and can be associated with high-grade and stage disease.[26] Therefore, an atypical appearance of a large encapsulated PZ lesion, especially one that does not appear to be contiguous with the TZ, should raise suspicion (►**Fig. 9G–K**).

- *Prostatic calcifications*: Incidence and degree of calcifications within the prostate gland increase with age, and they are prevalent after 50 years of age. They can be idiopathic or secondary to prostatitis, BPH, trauma (including iatrogenic such urethral stents or radiation therapy), diabetes mellitus, or even PCa.[27] They are most often believed to arise from the calcification of the corpora amylacea that, in turn, may be related at least in part to the prostatic secretions. Prostatic calcifications are often more easily visualized on computed tomography (CT) than on MRI. When seen on MRI, they exhibit signal void on all sequences due to the diamagnetic effect of these calcifications. The resulting marked hypointensity on T2WI and ADC can mimic csPCa within the TZ or PZ.

Pearls

In addition to the dark signal on T2WI and ADC, these calcifications appear dark on DWI at all *b*-values, suggesting their true nature. Moreover, they exhibit a complete absence of enhancement. While these calcifications can be solitary, they occur more often in clusters, which can be an additional clue to their presence. Correlation with CT, if available, can be conclusive in their characterization (►**Fig. 10**).

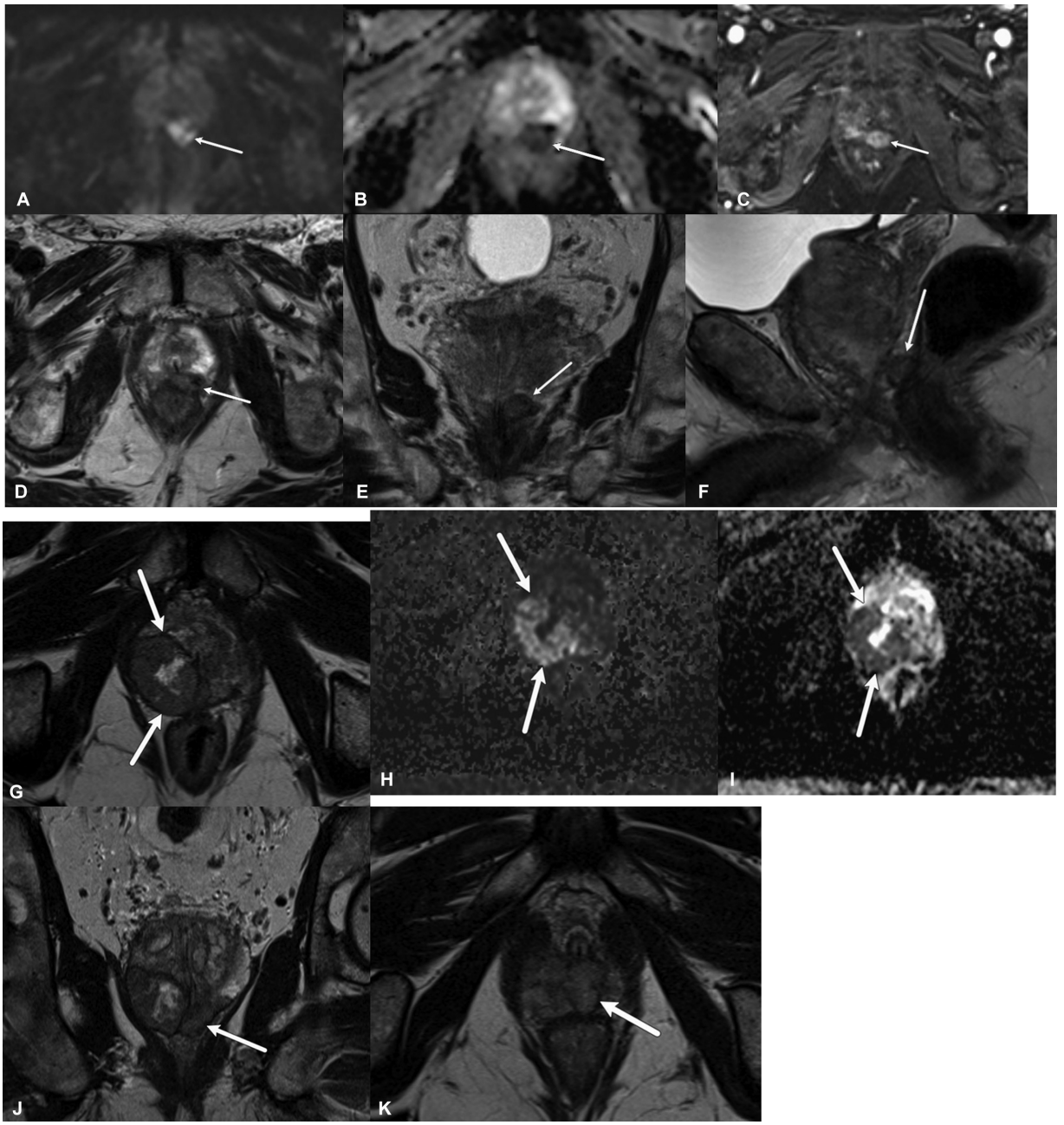

Fig. 9 (**A-F**) A focal lesion in the left apical peripheral zone (PZ) exhibits (**A**) marked hyperintensity on high *b*-value diffusion-weighted imaging (DWI; *arrow*) and (**B**) marked hypointensity on apparent diffusion coefficient (ADC; *arrow*), (**C**) with early dynamic contrast enhancement, meeting Prostate Imaging Reporting and Data System 4 (PI-RADS 4) criteria. (**D**) Corresponding hypointense signal abnormality on axial T2-weighted image (T2WI (*arrow*) shows hyperintense foci. Moreover, there is a capsule surrounding the nodule with continuity of the focal signal abnormality with the transitional zone (TZ), better seen on the (**E**) coronal (*arrow*) and (**F**) sagittal T2WI (*arrow*). These findings suggest extruded benign prostatic hyperplasia (BPH) nodule in this otherwise PI-RADS 4 lesion that showed benign prostatic tissue on a subsequent biopsy. (**G**) In another patient, axial T2WI shows a large moderately hypointense focal lesion involving most of the right PZ surrounded by a thin rim of low T2 signal intensity, giving the appearance of an extruded BPH nodule. However, some atypical features exist, as the nodule is not completely encapsulated. The lesion also has marked associated diffusion restriction on (**H**) high *b*-value DWI (*arrow*) and (**I**) ADC map (*arrow*). (**J**) Coronal T2WI and (**K**) axial T2WI show additional extension of the lesion crossing midline to the left posteromedial peripheral zone at the

FPs Related to Normal Anatomical Structures

- *Central zone (CZ)*: This normal symmetric cone-shaped region of prostatic tissue surrounding the ejaculatory ducts extends from the posteromedial base to mid-gland PZ, where ejaculatory ducts open into the urethra at the verumontanum. It can be seen in up to 80% of the patients and appears hypointense on T2WI and ADC, with mild DWI hyperintensity. Given this appearance, it can mimic csPCa[28] arising from PZ (given the hypointensity on ADC)

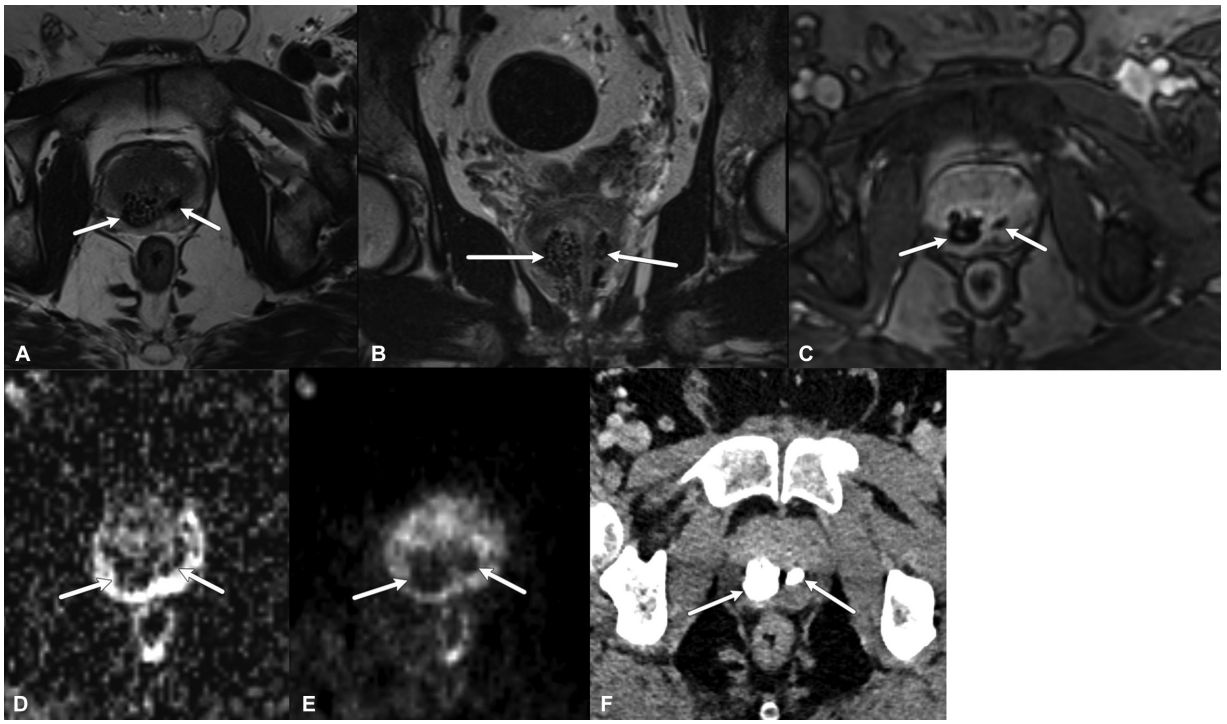

Fig. 10 Heterogeneous areas of signal loss on (**A**) axial (*arrows*) and (**B**) coronal (*arrows*) T2-weighted image (T2WI) within the posterior right greater than the left transition zone, with (**C**) a complete absence of enhancement on DCE (*arrows*). A corresponding dark signal on (**D**) apparent diffusion coefficient (ADC; *arrows*) and (**E**) high *b*-value diffusion-weighted imaging (DWI; *arrows*) suggest signal void rather than true diffusion restriction. (**F**) Correlation with computed tomography (CT) confirmed corresponding calcifications (*arrows*).

or TZ (given the hypointensity on T2WI). Assessing this structure can sometimes present a challenge to even experienced radiologists.

Pearls

A typical symmetric appearance of the CZ at the posterior prostate base and mid-gland, with no early arterial enhancement on DCE, helps differentiate this normal structure from PCa (►**Fig. 11A–D**). Also, look for a mustache or dumbbell shape on the axial images, a teardrop or triangular shape on coronal images, and the typical location surrounding the ejaculatory ducts in the posteromedial base to the mid-gland PZ.

CZ accounts for less than 5% of PCa cases. Focal early enhancement within the CZ or an asymmetry between the CZ on T2WI, ADC maps, or high *b*-value DWI that cannot be attributed to BPH should raise suspicion for PCa[29] (►**Fig. 11E–H**).

- *Anterior fibromuscular stroma (AFS)*: This tissue layer in the anterior prostate lacks glandular tissue and thus cannot give rise to PCa. Typically, it exhibits bilateral symmetry with a crescentic shape and appears as a hypointense region on T2WI, similar to pelvic floor musculature. There is no diffusion restriction, exhibiting hypointensity on both DWI and ADC map, with absent early arterial enhancement. In certain cases, AFS may show thickening, particularly in patients lacking significant TZ hypertrophy.

Pearls

Although PCa does not arise from AFS, cancer from PZ or TZ can involve AFS. Suspicious findings may appear hyperintense on T2WI and hypointense on ADC relative to pelvic floor musculature (typically more hypointense than the normal AFS), with hyperintensity on DWI. Other suspicious findings include focal masslike or asymmetric enlargement and early arterial enhancement. If this is suspected, the PI-RADS criteria should be applied utilizing the criteria for the respective zones from which the lesion is suspected to arise (►**Fig. 12**).

- *Thickened surgical/pseudo-capsule*: The prostatic surgical capsule, or pseudo-capsule, refers to the fibromuscular layer between the prostate's PZ and TZ. While this layer is loose and indistinct in normal prostate gland without BPH, it can be thickened in response to pressure from BPH nodules arising from the TZ.[30] On T2WI, it appears dark, and exhibits decreased ADC values, similar to csPCa.[31]

Pearls

A noteworthy characteristic is its bandlike or crescent-shaped appearance surrounding the TZ. Given the anatomical distortion of the ADC maps, the correlation of the hypointensity on the ADC map to the T2WI showing the typical appearance and location of the surgical capsule can be extremely helpful in preventing mislabeling this anatomical structure as csPCa (►**Fig. 13**).

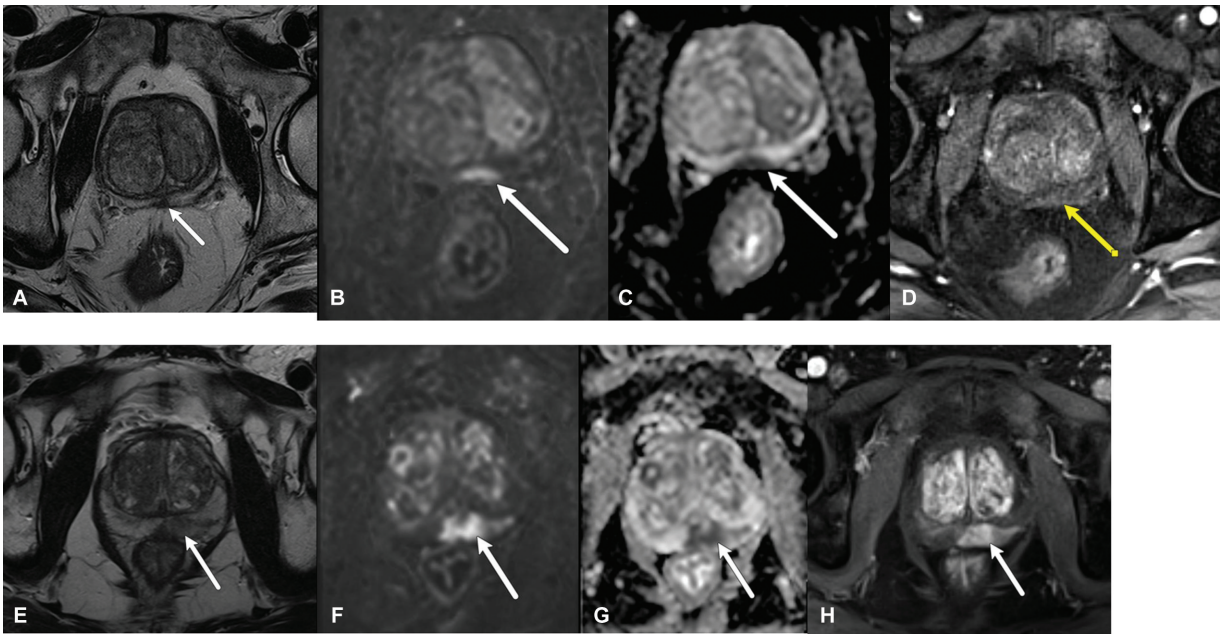

Fig. 11 (**A**) Axial T2-weighted image (T2WI; *arrow*) shows triangular hypointense area in the posterior midline peripheral zone (PZ) at the gland base with diffusion restriction on (**B**) high *b*-value diffusion-weighted imaging (DWI; *arrow*) and (**C**) apparent diffusion coefficient (ADC) map (*arrow*), (**D**) without early enhancement (*arrow*). This location and appearance are consistent with the normal central zone and should not be mistaken for a suspicious lesion, although it meets the criteria for a Prostate Imaging Reporting and Data System 4 (PI-RADS 4) lesion. Contrast this in another patient with (**E**) axial T2WI showing focal asymmetry in the left central zone (CZ) with a hypointense signal similar to the remaining CZ (*arrow*). The lesion also exhibits marked diffusion restriction on (**F**) high *b*-value DWI (*arrow*) and (**G**) ADC map (*arrow*). (**H**) Note the early arterial enhancement (*arrow*). Biopsy showed left prostate base Gleason score 3 + 4 adenocarcinoma.

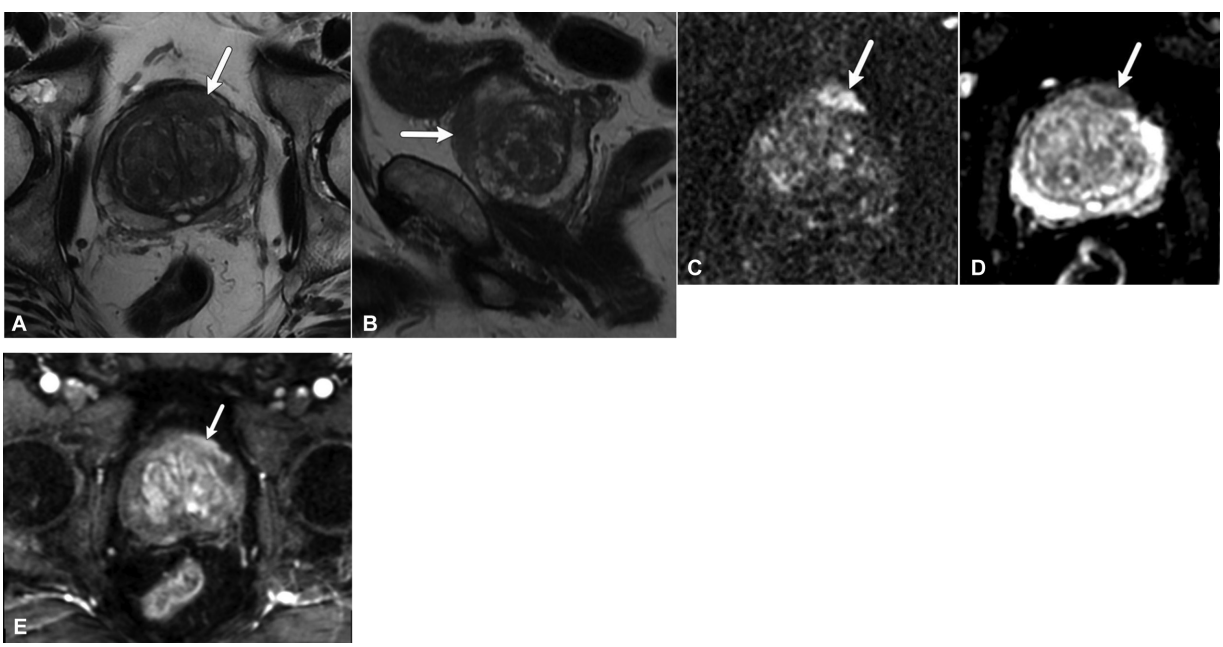

Fig. 12 (**A**) Axial (*arrow*) and (**B**) sagittal T2-weighted images (T2WIs; *arrow*) show focal masslike asymmetric enlargement of the left anterior fibromuscular stroma (AFS) appearing to arise from the left anterior peripheral zone (PZ). The lesion exhibits a T2 intermediate signal that is higher than the normal T2 dark AFS. There are corresponding areas of diffusion restriction with (**C**) marked hyperintensity on diffusion-weighted imaging (DWI; *arrow*) and (**D**) marked hypointensity apparent diffusion coefficient (ADC) map (*arrow*), with (**E**) asymmetric early arterial enhancement (*arrow*). This was suspicious for a Prostate Imaging Reporting and Data System 5 (PI-RADS 5) lesion from the left anterior prostate zone (PZ) invading the AFS. Subsequent radical prostatectomy revealed a Gleason score 4 + 3 prostatic adenocarcinoma mostly present in the left quadrants.

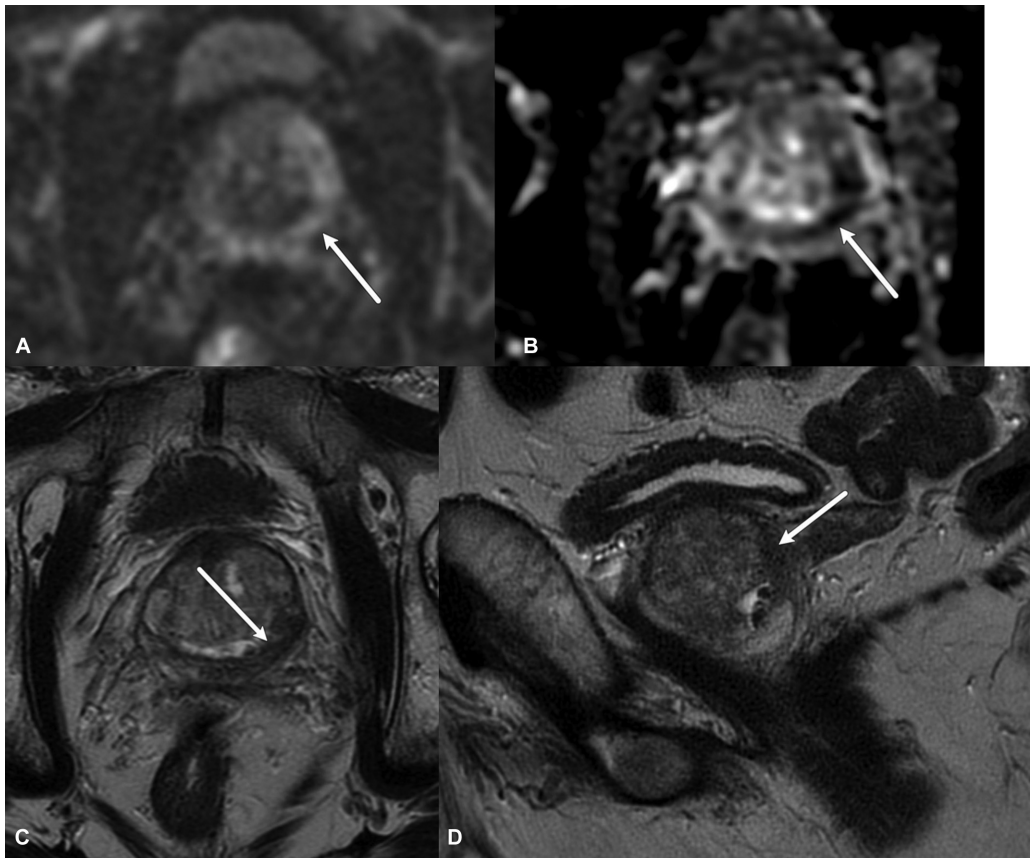

Fig. 13 A focal region in the left peripheral zone (PZ) appears mildly hyperintense on (**A**) high *b*-value diffusion-weighted imaging (DWI; *arrow*) and (**B**) markedly hypointense on apparent diffusion coefficient (ADC; *arrow*), raising suspicion for at least a Prostate Imaging Reporting and Data System 3 (PI-RADS 3) lesion. However, correlating with (**C**) axial and (**D**) sagittal T2-weighted image (T2WI), the lesion corresponds to the anatomical region of the surgical capsule between the transitional zone (TZ) and the prostate zone (PZ) with a crescent-shaped appearance (*arrow*), allowing more confident recognition as the thickened surgical capsule.

- *Neurovascular bundle*: The neurovascular bundles course along the posterolateral aspect of the prostate capsule on both sides, positioned at the 5 o'clock and 7 o'clock positions.[32] Due to its proximity to the PZ and imaging characteristics, including hypointensity/signal void on the T2WI and ADC map, the neurovascular bundle might be mistaken for a suspicious lesion within the PZ. It can also induce anatomical distortion of the prostate boundaries, potentially leading to misinterpretation as a mass lesion within the periprostatic space.

Pearls

The typical location along the posterolateral margins, a rounded contour on a single axial slice, tubular morphology across consecutive slices, and bilaterally symmetric bundles assist in resolving the suspicion.[33] The neurovascular bundles are often better assessed on T1WI, where they are recognized as oval (when viewed axially) or linear (when viewed in the long axis), hypointense structures surrounded by hyperintense fat. Neurovascular bundle invasion on T1WI may appear as asymmetric enlargement with loss of the intervening periprostatic fat plane or as gross tumor extension.[34]

- *Periprostatic venous plexus*: The periprostatic venous plexus is located close to the prostate capsule, and distinguishing it from the PZ on mpMRI can occasionally present a challenge due to low SI related to flow void on T2WI. Occasionally, it may also exhibit mildly restricted diffusion on EPI (►**Fig. 14**), and along with focal enhancement indicating abnormal enhancement kinetic, these findings may mimic csPCa.

Pearls

Awareness of the presence and expected location of this normal anatomical structure around the prostate should lead to evaluating the postcontrast sequence. Delayed enhancement would then point toward a periprostatic venous structure instead of a tumor.[35]

FPs Related to Postintervention Changes

- *Postbiopsy hemorrhage*: Often, patients with suspected PCa have undergone prostate biopsy before MRI evaluation. This may cause hemorrhage, producing MRI signal abnormalities within the prostate. Hemorrhage-related signal changes include, more commonly, T2 hypointensity, but

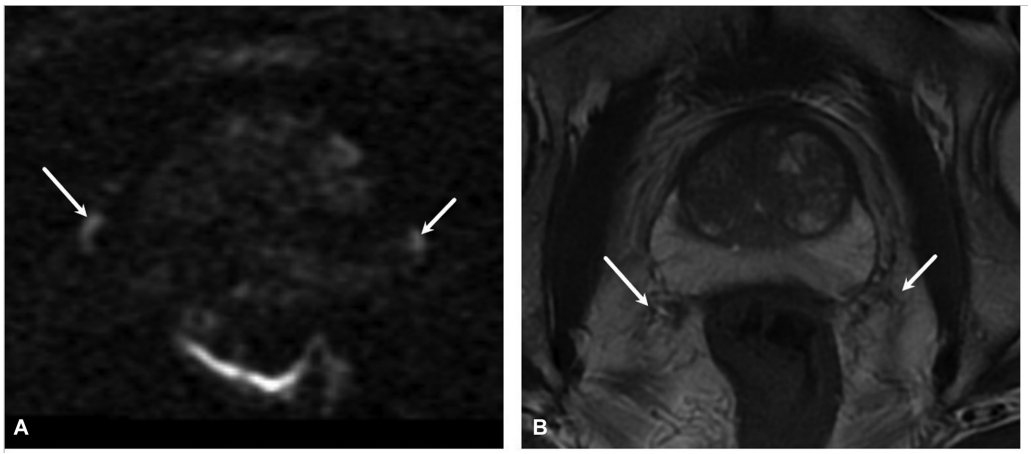

Fig. 14 Diffusion restriction is noted along the lateral margins of the bilateral peripheral zone (PZ) on (**A**) the high *b*-value diffusion-weighted imaging (DWI; *arrows*). (**B**) On correlating with T2-weighted image (T2WI; *arrows*), this corresponds to the bilateral periprostatic venous plexus.

depending on the age of the hemorrhage, they can also appear to restrict diffusion.[36] These changes overlap with the appearance of PCa on T2WI and DWI/ADC. Moreover, the T1 hyperintense appearance of the hemorrhage can interfere with assessing the region on DCE, wherein a tumor would be expected to demonstrate early enhancement.

The normal prostate gland produces citrate, which possesses anticoagulant properties. Consequently, the hemorrhage occurring after a biopsy is more extensive and lingers longer in the region of the normal PZ.[37] On the other hand, citrate levels are diminished in the areas affected by PCa,[38] resulting in a more rapid resolution of hemorrhage in the tumor due to the absence of the anticoagulant effect.[39]

Pearls

It is recommended to perform mpMRI at least 6 to 8 weeks after the biopsy to allow resolution of the hemorrhage, although hemorrhage-related changes can persist for up to 4.5 months.[40] csPCa exhibits more discrete masslike abnormality, demonstrating more marked SI alterations on DWI and DCE than postbiopsy hemorrhage. The hemorrhage exclusion sign can be helpful and describes the presence on T1W images of either a well-defined area of hypointensity in the PZ surrounded by an area of hyperintensity on at least one side or diffuse hyperintensity within a PZ region with an abrupt cutoff outlining a lesion. When this sign is present with a corresponding area of hypointensity on T2WI, it can strongly suggest csPCa[36] (►**Fig. 15**). T1WI subtraction postcontrast images or perfusion maps can help differentiate actual enhancing lesion from intrinsically T1 hyperintense hemorrhagic focus.

- *Postprostatic urethral lift (UroLift) procedure*: One of the newer minimally invasive approaches to treat symptomatic BPH includes a prostatic urethral lift with a UroLift procedure. It involves permanent metallic implants that retract the prostatic tissue, creating a channel for urine passage.[41] This MRI conditional device is safe for use with field strengths of up to 3 T.[42] However, it causes artifacts that negatively affect the MRI quality, with a recent study demonstrating obscuration of a third of the gland on DWI.[43]

Pearls

The potential to significantly affect the evaluation for PCa with MRI should be a part of the preprocedure discussion with the patient. A baseline MRI prior to the UroLift procedure to assess for PCa could also be considered. On MRI following a prior UroLift procedure, the UroLift device should not be mistaken for other linear metallic prostate implants utilized in PCa management. Brachytherapy seeds are usually more numerous than the UroLift tabs with distribution throughout the prostate, unlike UroLift tabs that are ideally placed anterolaterally at the 10 o'clock and 2 o'clock positions in the prostate (►**Fig. 16**). Fiducial markers used in external beam radiation therapy for PCa are similar in number to UroLift tabs but are shorter and thicker when compared to UroLift tabs.[43]

Pitfalls during Staging

- *Assessment of extra-prostatic extension (EPE)*: EPE assessment is crucial preoperatively due to its association with prognosis after radical prostatectomy and for deciding whether to spare the neurovascular bundles at surgery.[44,45] A newly proposed MRI-based EPE grading system showed an accuracy of 77 to 81%.[44,46] This is a three-tier system with grade 0 defined as having no suspicion of pathologic EPE; grade 1 with either capsular contact length (CCL) of $\geq$15 mm or capsular irregularity/bulge; grade 2 with both CCL of $\geq$15 mm and capsular irregularity/bulge; and grade 3 with frank EPE visible at MRI. Other specific findings of EPE include asymmetry/thickening of the neurovascular bundle and blunting of the rectoprostatic angle. However, several pitfalls exist that require careful consideration.

Pearls

A low threshold for suspecting EPE is recommended, particularly at the apex, where the lack of a capsule poses a higher risk. Apical lesions have implications for radiation therapy,

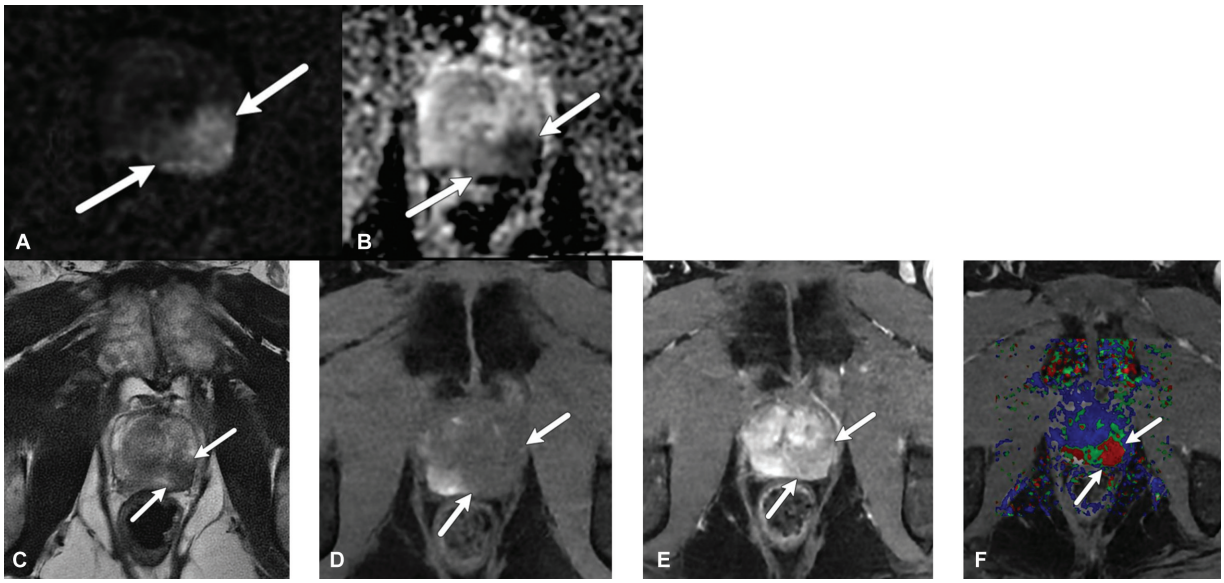

Fig. 15 A focal lesion in the left peripheral zone (PZ) exhibiting (**A**) marked hyperintensity on high *b*-value diffusion-weighted imaging (DWI; *arrows*) and (**B**) marked hypointensity on apparent diffusion coefficient (ADC) map (*arrows*), (**C**) with patchy areas of homogenous moderate hypointensity on T2-weighted image (T2WI) that are nonspecific in the setting of recent biopsy. (**D**) On pre-T1WI, a diffuse hyperintense region of hemorrhage is present throughout the right prostate zone (PZ), with an abrupt cutoff to a region of no hemorrhage (*arrows*, hemorrhage exclusion sign) and corresponding focal moderate hypointensity on T2WI (*arrows* in **C**), increasing confidence for cancer detection. Note that DCE assessment of the focal lesion was limited by the abutting regions of (**E**) intrinsic T1 hyperintensity (*arrows*), (**F**) but the perfusion map clearly shows positive DCE corresponding to the focal suspicious region (*red areas marked by arrows*). The lesion is thus Prostate Imaging Reporting and Data System 5 (PI-RADS 5). Prostate biopsy showed Gleason score 4 + 4 adenocarcinoma in the left apex and mid-gland with benign tissue in the right gland.

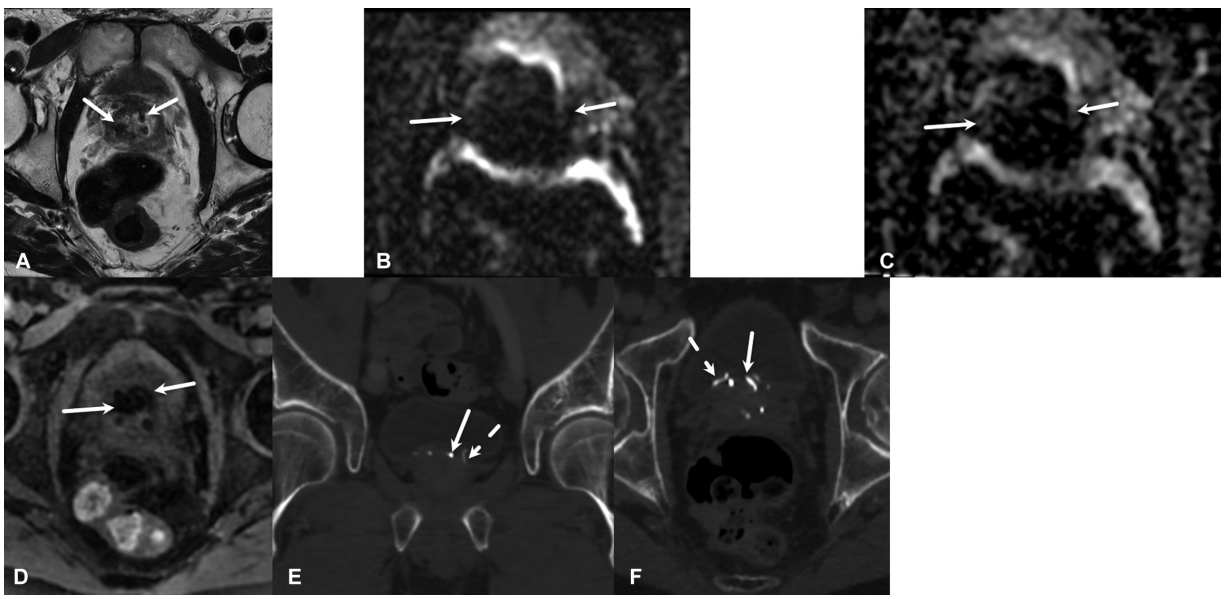

Fig. 16 (**A**) Axial T2-weighted image (T2WI; *arrows*) shows susceptibility artifacts in the transition zone (TZ) due to the stainless-steel inner tabs of the UroLift device; outer nitinol tabs are much less conspicuous with less susceptibility artifacts than inner tabs. (**B**) Corresponding diffusion-weighted imaging (DWI), (**C**) apparent diffusion coefficient (ADC) map, and (**D**) and axial in-phase T1WI show a larger degree of susceptibility artifact, with a large rounded signal void (*arrows*) almost obscuring the entire TZ, especially on diffusion imaging. (**E**) Coronal and (**F**) axial computed tomography (CT) images better demonstrate the device with inner stainless-steel tabs (*solid arrows*) exhibiting relatively greater attenuation than outer nitinol tabs (*dashed arrow*).

and are at risk of positive margins and recurrence after radical prostatectomy. Lesion proximity to the urethra should also be noted since urethral invasion is a concern (PI-RADS 5) and poses a surgical risk of injury to the external urinary sphincter, affecting urinary competence (►**Fig. 17**).

It should be remembered that MRI underestimates tumor boundaries compared to pathology,[47] with DCE performing better than T2WI and DWI for tumor volume estimation.

T2WI is key for evaluating a seminal vesicle (SV) that typically demonstrates a high signal on T2WI when

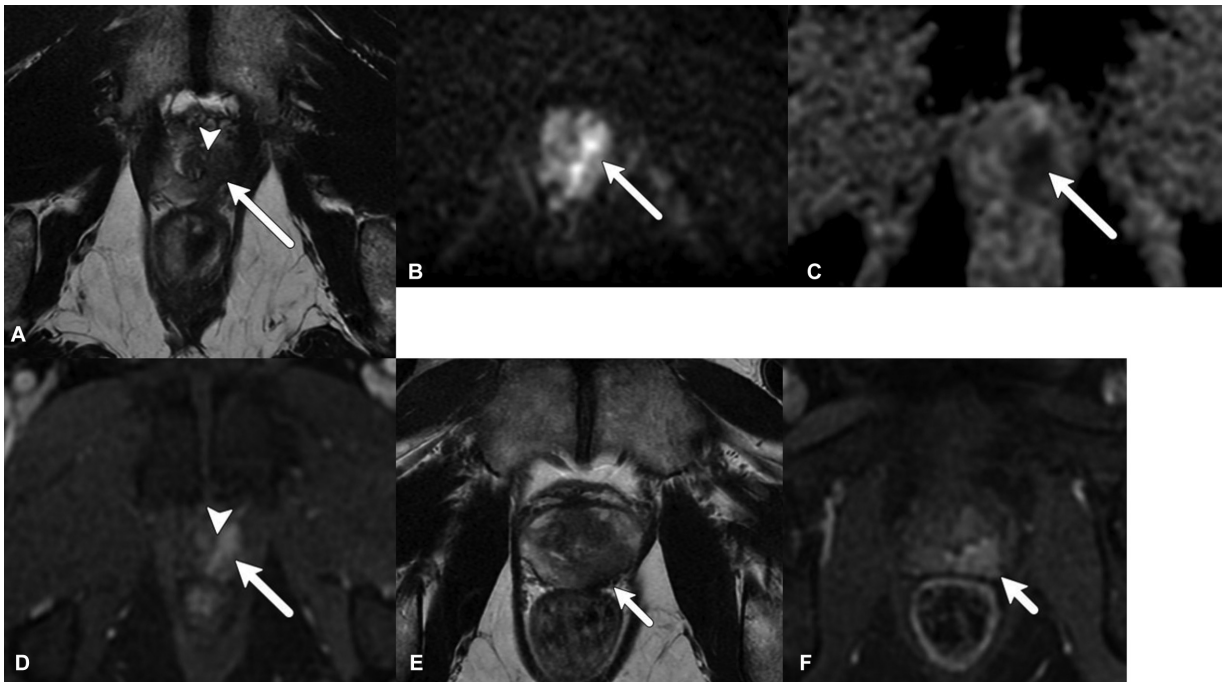

Fig. 17 (**A**) Axial T2-weighted image (T2WI) shows a moderately hypointense focal lesion (*arrow*) in the left apical peripheral zone. The lesion is markedly diffusion restricted on high *b*-value (**B**) diffusion-weighted imaging (DWI; *arrow*) and (**C**) apparent diffusion coefficient (ADC) map (*arrow*), and (**D**) dynamic contrast enhancement is positive (*arrow*). Slightly higher (**E**) axial T2WI (*arrow*) shows evidence of extraprostatic extension into the posterior periprostatic fat with asymmetric thickening and (**F**) enhancement of the left neurovascular bundle (*arrow*). The lesion involves the prostatic urethra and the external sphincter (*arrowheads* in **A** and **D**). This lesion is thus Prostate Imaging Reporting and Data System 5 (PI-RADS 5).

distended with seminal fluid. SV invasion, either as tumor growth along the SV or extension from the prostate base, defines the T3b TNM stage. Tumor infiltration or focal tumor deposits exhibit T2 hypointensity.[48] However, caution must be exercised as nondistended SV (such as from recent ejaculation) or benign pathologies, including inflammation and related amyloidosis,[49] can falsely mimic invasion on T2WI due to a dark signal (►**Fig. 18A–E**). Corresponding diffusion restriction and focal enhancement can increase confidence in characterizing T2 signal abnormality as pathologic (►**Fig. 18F–J**).

- *Lymph node assessment*: Pelvic lymph node dissection (PLND) is the most reliable method for documenting nodal invasion.[50] Prostate MRI allows pelvic and retroperitoneal lymph node evaluation for metastatic involvement but relies solely on morphological features. A common criterion for identifying metastatic pelvic nodes

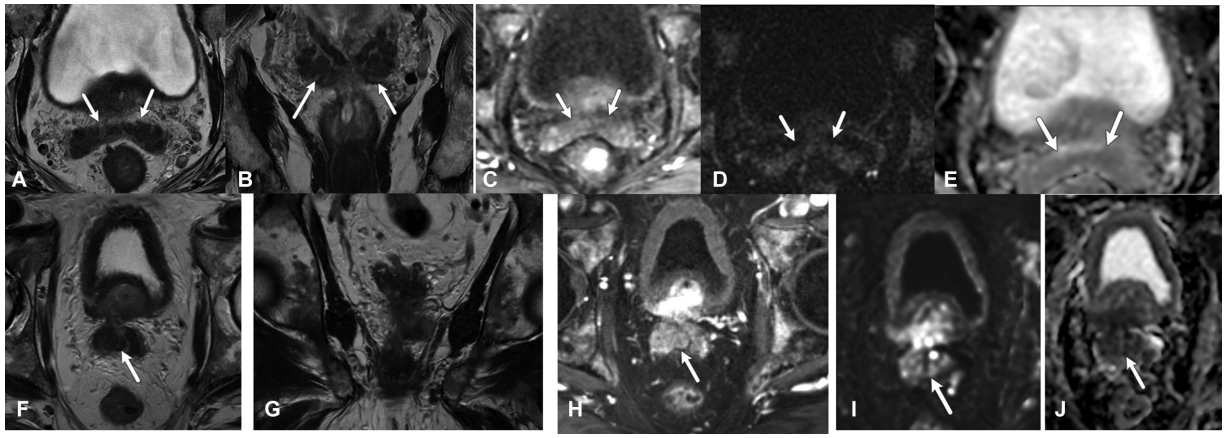

Fig. 18 (**A**) Axial (*arrows*) and (**B**) coronal T2-weighted images (T2WIs; *arrows*) demonstrate diffuse T2 hypointensity of the seminal vesicles in this patient with Gleason 3 + 3 disease in the peripheral zone (PZ; not shown). The appearance of the seminal vesicles is characteristic of amyloidosis, which was noted on a prior prostate biopsy. Note the (**C**) absence of enhancement (*arrows*) and (**D,E**) diffusion restriction (*arrows*) in the region of seminal vesicle signal abnormality. In contrast, in a different patient, (**F**) axial (*arrow*) and (**G**) coronal T2WI (*arrow*) show irregular T2 hypointense regions within the right greater than the left seminal vesicles. There are corresponding areas of (**H**) enhancement (*arrow*) and (**I,J**) diffusion restriction (*arrow*) concerning seminal vesicle extension in this biopsy-proven Gleason 5 + 4 disease involving the bilateral prostate base (not shown).

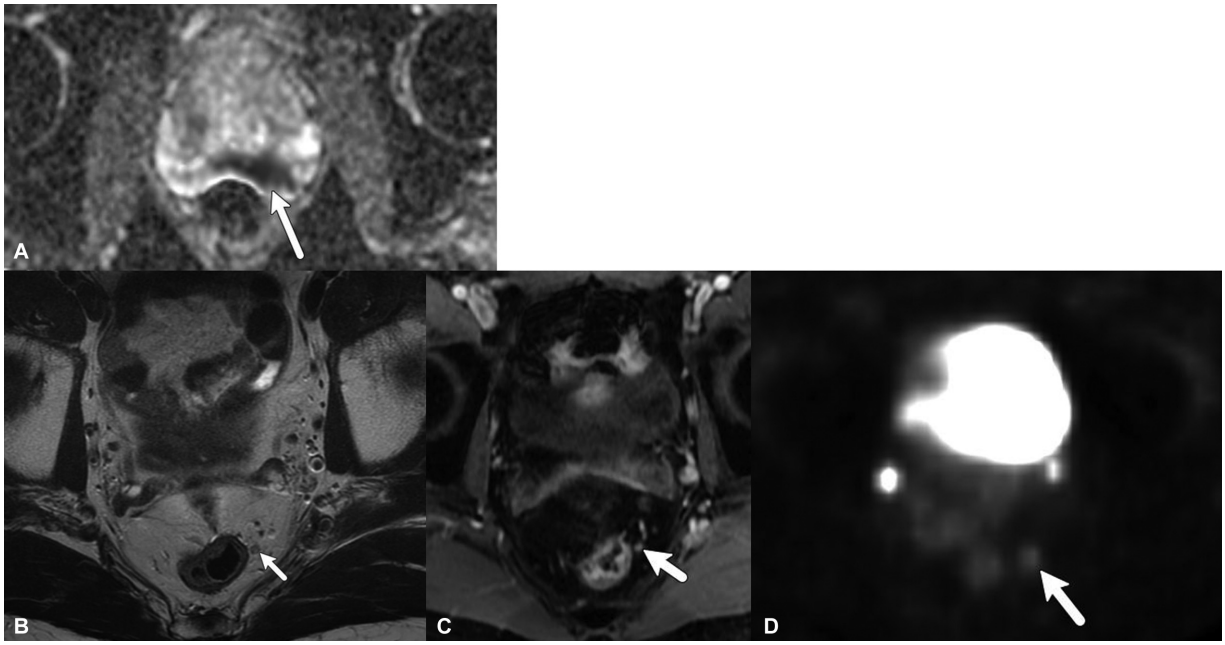

Fig. 19 (**A**) Apparent diffusion coefficient (ADC) map (*arrow*) shows markedly diffusion restricting Prostate Imaging Reporting and Data System 5 (PI-RADS 5) lesion in the left peripheral zone (PZ) with biopsy showing Gleason 4 + 5 adenocarcinoma. (**B**) Axial T2-weighted image (T2WI; *arrow*) and (**C**) contrast-enhanced T1WI (*arrow*) show a 0.4-cm rounded perirectal lymph node, which, although not suspicious by the magnetic resonance (MR) size criteria, was suspicious for (**D**) metastasis on prostate-specific membrane antigen (PSMA; piflufolastat F-18) positron emission tomography (PET; *arrow*).

is a short-axis diameter greater than 0.8 cm. A meta-analysis utilizing size criteria of short-axis diameter greater than 1 cm for oval and greater than 0.8 cm for round nodes with cross-sectional imaging demonstrated a pooled sensitivity of around 39 to 42% and a specificity of 82% for detecting positive nodes.[51] Nevertheless, metastatic and benign reactive lymph nodes show significant overlap in size (►**Fig. 19**).

Pearls

Other morphological signs of malignancy may be helpful, including irregular borders indicating extranodal extension,

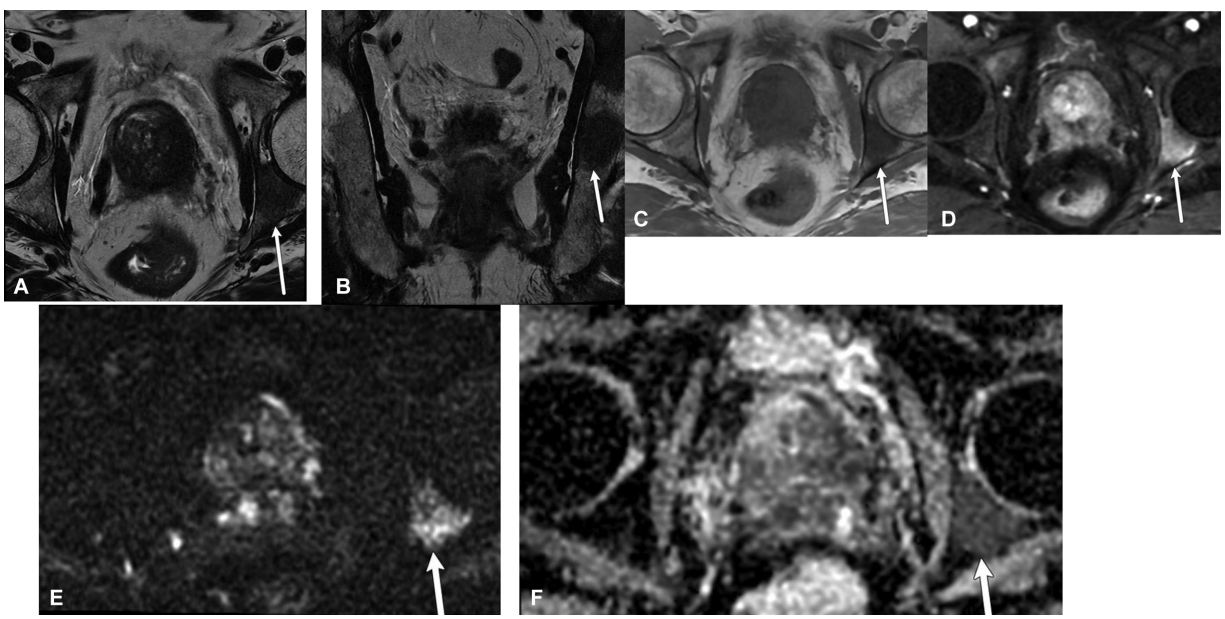

Fig. 20 (**A**) Axial and (**B**) coronal T2-weighted (T2W) images show a hypointense focal marrow replacing lesion involving the left acetabulum (*arrow*). (**C**) On T1WI (*arrow*), the lesion exhibits homogenous hypointensity to a greater degree than adjacent skeletal muscles. The lesion also exhibits strong enhancement on (**D**) the postcontrast image (*arrow*) and (**E**) diffusion restriction on diffusion-weighted imaging (DWI; *arrow*) and (**F**) apparent diffusion coefficient (ADC) map (*arrow*), which is highly suspicious for metastasis.

a round or irregular shape, and the absence of a fatty hilum.[52] A combination of morphological criteria and a DWI sequence demonstrated a specificity of 94% and sensitivity of 41% for detecting lymph node metastasis.[53] While malignant nodes may exhibit lower ADC values than benign nodes, overlap of their ADC values limits clinical utility.[54]

- *Bone assessment*: Bone is the second most common site of early metastases after lymph nodes.[55] Traditional bone scans have limited sensitivity and a high FN rate of up to 40%. Whole-body MRI with DWI has demonstrated greater accuracy than bone scans in detecting bone metastases.[56] Routine prostate MRI can also effectively detect bone metastases,[57] given that most PCa metastases arise within the pelvis and lumbar spine, often covered on prostate MRI.

Pearls

Bone metastases exhibit hypointensity on T1WI, intermediate- to hypointensity on T2WI, hyperintensity on DWI, and early, robust enhancement on DCE (►**Fig. 20**). MRI should be interpreted in the context of the PSA, Gleason score, and clinical stage to enhance metastatic detection and avoid unnecessary investigation of benign bone lesions, including hyperplastic hematopoietic bone marrow islands.[58] The

Table 1 Pitfalls in using PI-RADS for imaging analysis

False-negative pitfalls	Pearl
1. Susceptibility and motion artifacts	• Swap phase and frequency direction • Good bowel preparation prior to the examination • Antispasmodic agents • Using 1.5 T in patients with pelvic metal prosthesis • PSA values
2. Improper high *b*-value selection on high DWI images	• Use high value $\geq$1,400 s/mm^2 • Preferably greater than 1,600 s/mm^2 • Prefer not to use high-value DWI for ADC map generation
3. Suboptimal viewing of DWI/ADC	• Manually adjust the optimal viewing window level and width to enhance the contrast-to-noise ratio between normal glandular tissue and tumor
4. Improper use of endorectal coil	• Try to perform the examination with optimized parameters without using the endorectal coil whenever possible • When used, proper positioning of the coil is very important
5. Unusual pathologic variants of prostate cancer	• The reader should be familiar with the imaging appearance of the pathologic variant of primary adenocarcinoma • These entities should be suspected based on imaging appearance even in light of noncongruent PSA values
False-positive pitfalls	**Pearl**
1. Prostatitis	• Look for typical imaging patterns that suggest inflammation; segmental, linear, or wedge-shaped sharply marginated areas of abnormality • No significant change from the prior examination with negative fusion biopsy on the prior examination
2. Granulomatous prostatitis	• History of BCG therapy for superficial bladder cancer • Ringlike enhancement on postcontrast images
3. Stromal BPH nodule in TZ	• Look for well-demarcated margins and capsules • Symmetric enhancement compared to the rest of the TZ
4. Extruded BPH nodules in PZ	• Presence of well-demarcated capsule; maintained continuity with TZ if present
5. Prostatic calcification	• Usually dark on T2 and DWI • Absence of enhancement • CT correlation useful
6. Central zone	• Symmetric areas of restricted diffusion in classic location underlying the seminal vesicles • Typical morphology on T2-weighted images
7. Thickened surgical/pseudocapsule	• Although bandlike pattern can be seen on T2, if there is asymmetric diffusion restriction, attention needs to be given during biopsy
8. Restricted diffusion in neurovascular bundle or periprostatic venous plexus	• Typical location of neurovascular bundle and usually symmetric • Venous plexus has the corresponding abnormality seen on enhanced images
9. Postbiopsy hemorrhage	• Typical T1 hyperintense signal

Abbreviations: ADC, apparent diffusion coefficient; BCG, bacillus Calmette–Guerin; CT, computed tomography; DWI, diffusion-weighted imaging; PI-RADS, Prostate Imaging Reporting and Data System; PSA, prostate-specific antigen; TZ, transitional zone.

presence of intralesional fat is associated with benignity and can be helpful. Prostate MRI assessment of bone metastases is limited by restricted coverage and varying image acquisition protocols compared to musculoskeletal MRI (e.g., non-inclusion of short tau inversion recovery [STIR] on mpMRI of the prostate). Depending on the institutional protocol, bone lesions may often need to be primarily addressed in the large field-of-view T1WI, while T2WI, DWI, and DCE sequences concentrate on the prostate and SVs for optimal anatomical detail.[59]

Summary

In conclusion, while the PI-RADS scoring system utilizing mpMRI has revolutionized the management of PCa, it is essential to acknowledge the limitations and pitfalls of this technique. Understanding and addressing these challenges and ongoing refinements to this system can improve utility and accuracy in detecting csPca. A summary of common entities causing FN and FP findings is summarized in ►**Table 1**.

Funding
None.

Conflict of Interest
None declared.

References

1 Barentsz JO, Richenberg J, Clements R, et al; European Society of Urogenital Radiology. ESUR prostate MR guidelines 2012. Eur Radiol 2012;22(04):746–757
2 Turkbey B, Rosenkrantz AB, Haider MA, et al. Prostate Imaging Reporting and Data System Version 2.1: 2019 Update of Prostate Imaging Reporting and Data System Version 2. Eur Urol 2019;76 (03):340–351
3 Becerra MF, Alameddine M, Zucker I, et al. Performance of multiparametric MRI of the prostate in biopsy naïve men: a meta-analysis of prospective studies. Urology 2020;146:189–195
4 Westphalen AC, McCulloch CE, Anaokar JM, et al. Variability of the positive predictive value of PI-RADS for prostate MRI across 26 centers: experience of the Society of Abdominal Radiology Prostate Cancer Disease-focused Panel. Radiology 2020;296(01):76–84
5 Moldovan PC, Van den Broeck T, Sylvester R, et al. What is the negative predictive value of multiparametric magnetic resonance imaging in excluding prostate cancer at biopsy? A systematic review and meta-analysis from the European Association of Urology Prostate Cancer Guidelines Panel. Eur Urol 2017;72(02):250–266
6 Sundaram KM, Rosenberg J, Syed AB, Chang ST, Loening AM. Assessment of T2-weighted image quality at prostate MRI in patients with and those without intramuscular injection of glucagon. Radiol Imaging Cancer 2023;5(03):e220070
7 Metens T, Miranda D, Absil J, Matos C. What is the optimal b value in diffusion-weighted MR imaging to depict prostate cancer at 3T? Eur Radiol 2012;22(03):703–709
8 Manetta R, Palumbo P, Gianneramo C, et al. Correlation between ADC values and Gleason score in evaluation of prostate cancer: multicentre experience and review of the literature. Gland Surg 2019;8(Suppl 3):S216–S222
9 Fine SW. Variants and unusual patterns of prostate cancer: clinicopathologic and differential diagnostic considerations. Adv Anat Pathol 2012;19(04):204–216
10 Yamada K, Kozawa N, Nagano H, Fujita M, Yamada K. MRI features of mucinous adenocarcinoma of the prostate: report of four cases. Abdom Radiol (NY) 2019;44(04):1261–1268
11 Westphalen AC, Coakley FV, Kurhanewicz J, Reed G, Wang ZJ, Simko JP. Mucinous adenocarcinoma of the prostate: MRI and MR spectroscopy features. AJR Am J Roentgenol 2009;193(03): W238–W243
12 Truong M, Feng C, Hollenberg G, et al. A comprehensive analysis of cribriform morphology on magnetic resonance imaging/ultrasound fusion biopsy correlated with radical prostatectomy specimens. J Urol 2018;199(01):106–113
13 Seyrek N, Hollemans E, Schoots IG, van Leenders GJLH. Association of quantifiable prostate MRI parameters with any and large cribriform pattern in prostate cancer patients undergoing radical prostatectomy. Eur J Radiol 2023;166:110966
14 Hoeks CMA, Barentsz JO, Hambrock T, et al. Prostate cancer: multiparametric MR imaging for detection, localization, and staging. Radiology 2011;261(01):46–66
15 Rais-Bahrami S, Nix JW, Turkbey B, et al. Clinical and multiparametric MRI signatures of granulomatous prostatitis. Abdom Radiol (NY) 2017;42(07):1956–1962
16 Bour L, Schull A, Delongchamps NB, et al. Multiparametric MRI features of granulomatous prostatitis and tubercular prostate abscess. Diagn Interv Imaging 2013;94(01):84–90
17 Hosseinzadeh K, Schwarz SD. Endorectal diffusion-weighted imaging in prostate cancer to differentiate malignant and benign peripheral zone tissue. J Magn Reson Imaging 2004;20(04): 654–661
18 Berry SJ, Coffey DS, Walsh PC, Ewing LL. The development of human benign prostatic hyperplasia with age. J Urol 1984;132 (03):474–479
19 Guneyli S, Ward E, Thomas S, et al. Magnetic resonance imaging of benign prostatic hyperplasia. Diagn Interv Radiol 2016;22(03): 215–219
20 Ling D, Lee JKT, Heiken JP, Balfe DM, Glazer HS, McClennan BL. Prostatic carcinoma and benign prostatic hyperplasia: inability of MR imaging to distinguish between the two diseases. Radiology 1986;158(01):103–107
21 Li H, Sugimura K, Kaji Y, et al. Conventional MRI capabilities in the diagnosis of prostate cancer in the transition zone. AJR Am J Roentgenol 2006;186(03):729–742
22 McNeal JE, Redwine EA, Freiha FS, Stamey TA. Zonal distribution of prostatic adenocarcinoma. Correlation with histologic pattern and direction of spread. Am J Surg Pathol 1988;12(12):897–906
23 Schieda N, Lim CS, Zabihollahy F, et al. Quantitative prostate MRI. J Magn Reson Imaging 2021;53(06):1632–1645
24 Hoeks CMA, Hambrock T, Yakar D, et al. Transition zone prostate cancer: detection and localization with 3-T multiparametric MR imaging. Radiology 2013;266(01):207–217
25 Akin O, Sala E, Moskowitz CS, et al. Transition zone prostate cancers: features, detection, localization, and staging at endorectal MR imaging. Radiology 2006;239(03):784–792
26 Bonde AA, Korngold EK, Foster BR, et al. Prostate cancer with a pseudocapsule at MR imaging: a marker of high grade and stage disease? Clin Imaging 2016;40(03):365–369
27 Hong CG, Yoon BI, Choe HS, Ha US, Sohn DW, Cho YH. The prevalence and characteristic differences in prostatic calcification between health promotion center and urology department outpatients. Korean J Urol 2012;53(05):330–334
28 Vargas HA, Akin O, Franiel T, et al. Normal central zone of the prostate and central zone involvement by prostate cancer: clinical and MR imaging implications. Radiology 2012;262(03):894–902
29 Purysko AS, Baroni RH, Giganti F, et al. PI-RADS version 2.1: a critical review, from the AJR special series on radiology reporting and data systems. AJR Am J Roentgenol 2021;216(01):20–32
30 Semple JE. Surgical capsule of the benign enlargement of the prostate. Its development and action. BMJ 1963;1(5346):1640–1643

31 Rosenkrantz AB, Taneja SS. Radiologist, be aware: ten pitfalls that confound the interpretation of multiparametric prostate MRI. AJR Am J Roentgenol 2014;202(01):109–120
32 Guerra A, Flor-de-Lima B, Freire G, Lopes A, Cassis J. Radiologic-pathologic correlation of prostatic cancer extracapsular extension (ECE). Insights Imaging 2023;14(01):88
33 Panebianco V, Barchetti F, Barentsz J, et al. Pitfalls in interpreting mp-MRI of the prostate: a pictorial review with pathologic correlation. Insights Imaging 2015;6(06):611–630
34 Kundra V, Silverman PM, Matin SF, Choi H. Imaging in oncology from the University of Texas M. D. Anderson Cancer Center: diagnosis, staging, and surveillance of prostate cancer. AJR Am J Roentgenol 2007;189(04):830–844
35 Panebianco V, Giganti F, Kitzing YX, et al. An update of pitfalls in prostate mpMRI: a practical approach through the lens of PI-RADS v. 2 guidelines. Insights Imaging 2018;9(01):87–101
36 Rosenkrantz AB, Kopec M, Kong X, et al. Prostate cancer vs. post-biopsy hemorrhage: diagnosis with T2- and diffusion-weighted imaging. J Magn Reson Imaging 2010;31(06):1387–1394
37 Barrett T, Vargas HA, Akin O, Goldman DA, Hricak H. Value of the hemorrhage exclusion sign on T1-weighted prostate MR images for the detection of prostate cancer. Radiology 2012;263(03): 751–757
38 Zakian KL, Shukla-Dave A, Ackerstaff E, Hricak H, Koutcher JA. 1H magnetic resonance spectroscopy of prostate cancer: biomarkers for tumor characterization. Cancer Biomark 2008;4(4–5):263–276
39 Tamada T, Sone T, Jo Y, et al. Prostate cancer: relationships between postbiopsy hemorrhage and tumor detectability at MR diagnosis. Radiology 2008;248(02):531–539
40 White S, Hricak H, Forstner R, et al. Prostate cancer: effect of postbiopsy hemorrhage on interpretation of MR images. Radiology 1995;195(02):385–390
41 Das AK, Leong JY, Roehrborn CG. Office-based therapies for benign prostatic hyperplasia: a review and update. Can J Urol 2019;26(4, Suppl 1):2–7
42 NeoTract, Inc. UroLift® System UL400 Instructions for Use UroLift System UL400. Accessed February 23, 2024 at: https://in.urolift.-com/wp-content/uploads/2022/09/India-IFU-for-UroLift-System.pdf
43 Benidir T, Austhof E, Ward RD, et al. Impact of prostate urethral lift device on prostate magnetic resonance image quality. J Urol 2023; 209(04):JU0000000000003156
44 Park KJ, Kim MH, Kim JK. Extraprostatic tumor extension: comparison of preoperative multiparametric MRI criteria and histopathologic correlation after radical prostatectomy. Radiology 2020;296(01):87–95
45 Diaz TA, Benson B, Clinkenbeard A, Long JR, Kawashima A, Yano M. MRI evaluation of patients before and after interventions for benign prostatic hyperplasia: an update. AJR Am J Roentgenol 2022;218(01):88–99
46 Mehralivand S, Shih JH, Harmon S, et al. A grading system for the assessment of risk of extraprostatic extension of prostate cancer at multiparametric MRI. Radiology 2019;290(03):709–719
47 Le Nobin J, Rosenkrantz AB, Villers A, et al. Image guided focal therapy for magnetic resonance imaging visible prostate cancer: defining a 3-dimensional treatment margin based on magnetic resonance imaging histology co-registration analysis. J Urol 2015; 194(02):364–370
48 Soylu FN, Peng Y, Jiang Y, et al. Seminal vesicle invasion in prostate cancer: evaluation by using multiparametric endorectal MR imaging. Radiology 2013;267(03):797–806
49 Yang Z, Laird A, Monaghan A, Seywright M, Ahmad I, Leung HY. Incidental seminal vesicle amyloidosis observed in diagnostic prostate biopsies–are routine investigations for systemic amyloidosis warranted? Asian J Androl 2013;15(01):149–151
50 Sankineni S, Brown AM, Fascelli M, et al. Lymph node staging in prostate cancer. Curr Urol Rep 2015;16(05):30
51 Hövels AM, Heesakkers RAM, Adang EM, et al. The diagnostic accuracy of CT and MRI in the staging of pelvic lymph nodes in patients with prostate cancer: a meta-analysis. Clin Radiol 2008; 63(04):387–395
52 Pedersen CK, Babu AS. Understanding the lymphatics: an updated review of the N category of the AJCC 8th edition for urogenital cancers. AJR Am J Roentgenol 2021;217(02):368–377
53 Muteganya R, Goldman S, Aoun F, Roumeguère T, Albisinni S. Current imaging techniques for lymph node staging in prostate cancer: a review. Front Surg 2018;5:74
54 Thoeny HC, Froehlich JM, Triantafyllou M, et al. Metastases in normal-sized pelvic lymph nodes: detection with diffusion-weighted MR imaging. Radiology 2014;273(01):125–135
55 Kitajima K, Murphy RC, Nathan MA, et al. Detection of recurrent prostate cancer after radical prostatectomy: comparison of 11C-choline PET/CT with pelvic multiparametric MR imaging with endorectal coil. J Nucl Med 2014;55(02):223–232
56 Pasoglou V, Larbi A, Collette L, et al. One-step TNM staging of high-risk prostate cancer using magnetic resonance imaging (MRI): toward an upfront simplified "all-in-one" imaging approach? Prostate 2014;74(05):469–477
57 Woo S, Kim SY, Kim SH, Cho JY. Identification of bone metastasis with routine prostate MRI: a study of patients with newly diagnosed prostate cancer. AJR Am J Roentgenol 2016;206(06): 1156–1163
58 Tanaka T, Yang M, Froemming AT, et al. Current imaging techniques for and imaging spectrum of prostate cancer recurrence and metastasis: a pictorial review. Radiographics 2020;40(03): 709–726
59 Vargas HA, Schor-Bardach R, Long N, et al. Prostate cancer bone metastases on staging prostate MRI: prevalence and clinical features associated with their diagnosis. Abdom Radiol (NY) 2017;42(01):271–277

